

An Update of E03-004 to JLab-PAC29

Measurement of Single Target-Spin Asymmetry in Semi-Inclusive $n^\uparrow(e, e'\pi^-)$ Reaction on a Transversely Polarized ^3He Target

The Jefferson Lab Hall A Collaboration

D.J. Margaziotis

California State University–Los Angeles, Los Angeles, California.

W. Chen, D. Dutta, H. Gao, K. Kramer, X. Qian, Q. Ye, X. Zong

Triangle Universities Nuclear Laboratory, Duke University, Durham, North Carolina.

P. Markowitz

Florida International University, Miami, Florida.

M. Grosse-Perdekamp, D. Howell, A. Nathan, N. Makins, J.-C. Peng (Co-Spokesperson),
L. Zhu

University of Illinois, Urbana-Champaign, Illinois.

A. Afanasev, J.-P. Chen (Co-Spokesperson), E. Chudakov, A. Deur, R. Feuerbach,
J. Gomez, D.W. Higinbotham, J.O. Hansen, C. W. de Jager, M. K. Jones, J. LeRose,
W. Melnitchouk, R. Michaels, S. Nanda, B. Reitz, A. Saha, B. Wojtsekhowski
Jefferson Lab, Newport News, Virginia.

K. Allada, C. Dutta, A. Kolarkar, W. Korsch
University of Kentucky, Lexington, Kentucky.

F. Benmokhtar, J.J. Kelly, C.C. Chang
University of Maryland, College Park, Maryland.

K. Paschke
University of Massachusetts, Amherst, Massachusetts.

W. Bertozzi, S. Gilad, P. Monaghan, Y. Qiang, X. Zhan, X. Zheng
Massachusetts Institute of Technology, Cambridge, Massachusetts.

P. Ulmer, L. Weinstein
Old Dominion University, Norfolk, Virginia.

R. Gilman, C. Glashauser, X. Jiang (Co-Spokesperson) ^a, E. Kuchina, G. Kumbartzki,
E. Schulte, R. Ransome.

^aContact person, email: jiang@jlab.org

Rutgers University, Piscataway, New Jersey.

F. Butaru, Z.-E. Meziani, B. Sawatzky, P. Solvignon, H. Yao
Temple University, Philadelphia, Pennsylvania.

L. Gamberg
Pennsylvania State University at Berks, Reading, Pennsylvania.

G. Cates, R. Lindgren, N. Liyanage, V. Nelyubin, B. Norum, K. Slifer, K. Wang
University of Virginia, Charlottesville, Virginia.

T. Averett, T. Holmstrom, A. Kelleher, V. Sulkosky
College of William and Mary, Williamsburg, Virginia.

Y. Jiang, H. Lu, Y. Ye
University of Science and Technology of China, Hefei, P.R.China.

J. Yuan, S. Zhou
China Institute of Atomic Energy, Beijing, P.R.China.

B.-Q. Ma, Y.-J. Mao, H.-X. Ye
School of Physics, Beijing University, P.R. China.

Seonho Choi
Seoul National University, Seoul, Korea

J.R.M. Annand, D. Ireland, J.D. Kellie, K. Livingston, R. Kaiser, D. Protopopescu,
G. Rosner, D. Watts.
University of Glasgow, Glasgow, Scotland, United Kingdom.

E. Cisbani, F. Cusanno, S. Frullani, F. Garibaldi, M.L. Magliozzi, G. Urciuoli, M. Iodice,
R. De Leo, L. Lagamba, S. Marrone, E. Nappi
INFN Roma-I, INFN Roma-III, INFN Bari and University of Bari, Italy

M. Potokar, S. Širca
Jozef Stefan Institute, and University of Ljubljana, Ljubljana, Slovenia

A. J. Sarty
St. Mary's University, Halifax, Nova Scotia, Canada.

E. Piasetzky
Tel Aviv University, Tel Aviv, Israel

Abstract: This document is an update of the previously approved Hall A experiment E03-004. In this experiment, we plan to measure the target single spin asymmetry (SSA) in the semi-inclusive deep-inelastic $n^\uparrow(e, e'\pi^-)X$ reaction with a transversely polarized ^3He target. The goal of this experiment is to provide the first measurement of the neutron transverse target SSA complementary to the recent HERMES and COMPASS measurements on proton and deuteron. The recent results on SSA have generated great interest in the international hadronic physics community, as evidenced by the large number of recent workshops dedicated to the topic of SSA. SSA data on transversely polarized neutron will provide crucial new information on the flavor dependences of various structure and fragmentation functions probed by the SSA experiments. This first neutron measurement focuses on the valence quark region, $x = 0.13 \sim 0.41$, at $Q^2 = 1.31 \sim 3.1 \text{ GeV}^2$. This kinematics is comparable to the HERMES proton measurement, while COMPASS data are mostly in the low- x region. The variation of single spin asymmetry as a function of Collins and Sivers angles will provide a clear separation of the two competing mechanisms—the Sivers effect and the Collins effect. This is a crucial step toward the extraction of the quark transversity distributions in semi-inclusive deep-inelastic scattering. Data from this experiment, when combined with the world proton and deuteron data, will provide powerful constraints on the transversity distributions and Sivers function for both u -quark and d -quark in the valence region. A re-approval of 24 days of beam time at 6 GeV in Hall A with a high scientific rating is requested.

Contents

1	A summary of major developments since PAC23	6
2	Physics Motivation	7
2.1	Transverse target spin related SIDIS cross sections	12
2.2	Transverse target single-spin asymmetry	13
2.3	Factorization in SIDIS and recent JLab data	14
3	The Proposed Measurement	15
3.1	Overview	15
3.2	The choice of kinematics	17
3.3	Phase spaces, Collins angle and Sivers angle coverage	18
3.4	The experimental observable	22
3.5	The electron arm: BigBite	22
	Single particle background, BigBite single arm trigger and track re- construction	24
3.6	The hadron arm HRS _L and hadron PID	26
	The left-arm RICH detector	27
	An option of a pressurized gas Cherenkov vs. RICH	27
3.7	Trigger and offline event selection	29
3.8	Luminosity monitors	29
3.9	The polarized ³ He target	30
	Effects of BigBite magnetic field	33
4	Event Rate Estimate and Statistical Uncertainties	33
4.1	Cross section and rate estimate	33
4.2	Cross sections, rates and total number of ($e, e'\pi^-$) events	35
4.3	Statistical uncertainties of Collins and Sivers moments for π^- and K^- production	35
4.4	Systematic uncertainties	36
	Effective nucleon polarization in ³ He	36
	Corrections to A_{UT} due to target polarization drifts	37
	Pions from exclusive ρ production	37
	Other terms in SSA and cross sections	38
5	Beam time request, hardware costs and installation time needed	38
5.1	Beam time request	38
5.2	Hardware costs and installation time needed	39
6	Expected Results and Impacts	39
7	Relation with other experiments	42

8	Manpower and collaboration	43
9	Summary	44
10	Acknowledgment	44
A	Appendix-I. PAC23 report on E03-004	45
B	Appendix-II. Simulation of BigBite background rates and comparisons with test runs	46
C	Appendix-III. Separation of Collins and Sivers asymmetries	48

1 A summary of major developments since PAC23

- New HERMES data with a transversely polarized proton target clearly show non-zero Collins and Sivers moments. New COMPASS deuteron data show small (consistent with zero) Collins and Sivers asymmetries. These results suggest a strong and unexpected flavor dependence of both Collins and Sivers functions.
- For the first time, Collins fragmentation functions were studied with $e^+e^- \rightarrow \pi\pi$ data from Belle at KEK. The data show a significant azimuthal asymmetry attributed to the Collins function.
- There are rapid new theoretical development in the study and understanding of the SSA processes. In addition to model (such as quark-soliton models and di-quark models) calculations of the transversity distributions and lattice calculations of the tensor charges, increasingly large efforts have been devoted to understanding the reaction mechanisms of the SSA from the fundamental theory of strong interaction, QCD. In particular, the rapid progress in the study of the Sivers effect and related mechanisms has brought our understanding to a new level. The link of the SIDIS SSA with other area of hadronic physics, such as in the Drell-Yan and $p - \bar{p}$ reactions and multi-hadron production processes, has not only raised great interest in theoretical efforts, but also in experimental efforts. Transverse spin physics has become a major goal of a number of new facilities, including RHIC-spin, J-PARC in Japan, PAX at the future Facility for Anti-proton and Ion Research (FAIR) at GSI, JLab 12 GeV, and the future electron-ion collider (EIC).

Experimental developments:

- PAC23 was concerned with the applicability of factorization at JLab kinematics. Recent SIDIS data from Hall C and Hall B indicate naive x - z factorization is a reasonable approximation.
- This experiment concentrates on $z=0.5$. Updated estimates use calculated SIDIS rates that have been cross checked with recent Hall C E00-108 data. A full SIDIS physics Monte Carlo simulation code has been developed. We have optimized kinematics to favor current fragmentation and to have clear separation of Sivers and Collins moments.
- The BigBite spectrometer has been used to take data for the Short-Range-Correlation experiment and is ready to take beam for the G_E^n experiment in February, 2006. Background has been carefully studied with a full GEANT Monte-Carlo simulation which has been compared with several test run data.
- Rb-K hybrid ^3He target cells were demonstrated to have high polarization, short spin-up time, and much improved success rate in production. The fast

spin-flip technique has been worked out. Fringe field issue is fully under control. New optics with a fiber system makes the target system much more flexible and easier to install.

- Data from HAPPEX running demonstrated the adequacy of the HAPPEX Lumi detectors for our luminosity monitoring.
- HRS is robust for pion detection. To have kaon data as a by-product, the RICH detector will be re-installed. The RICH performed well during Hyper-nuclear and Penta-quark experiments, demonstrating a superb capability for K/π separation. The newly designed Heavy Gas Cherenkov for other experiments will be a back-up.

2 Physics Motivation

At leading twist, three parton distribution functions describe the momentum and spin of the quarks inside the nucleon. These are the quark density distribution $q(x, Q^2)$, the quark helicity distribution $\Delta q(x, Q^2)$, and the quark transversity distribution $\delta q(x, Q^2)$. Both $q(x, Q^2)$ and $\Delta q(x, Q^2)$ are quite well determined from DIS experiments. In contrast, $\delta q(x, Q^2)$ is practically unknown and remains a major frontier in our quest for understanding the spin structure of the nucleon.

Viewed in the helicity basis, the transversity distribution^{1,2} δq (or alternatively h_1^q) corresponds to the forward scattering amplitude involving helicity-flip of both quark and nucleon, i.e., $N \rightarrow q^{\leftarrow} \rightarrow N^{\leftarrow} q^{\rightarrow}$. This chirally-odd nature of δq prevents its measurement in inclusive DIS which conserves chirality. In the transverse spin basis, the transversity distribution is related to the probability of finding the quark transversely polarized along the same direction of a transversely polarized nucleon; $\delta q = q^{\uparrow\uparrow} - q^{\uparrow\downarrow}$. This is analogous to the helicity distribution which reflects the probability for a quark to have the same helicity as the nucleon; $\Delta q = q^{\rightarrow\rightarrow} - q^{\rightarrow\leftarrow}$. The differences between Δq and δq are expected as a result of the relativistic motion of the quarks for which boosts and rotations do not commute. Several model calculations on δq , based on chiral quark-soliton model³, PQCD model and quark-diquark model⁴ have been performed. A measurement of the transversity distribution would provide much insight on the dynamics of quarks in the nucleon.

Although the chirally-odd δq can not be measured in inclusive DIS, it can nevertheless be probed in processes which involve another chirally-odd quantity. One example is the Drell-Yan process involving two transversely polarized nucleons. Another process is the semi-inclusive DIS on a transversely polarized nucleon in which a chirally-odd fragmentation function, called Collins function⁵, can lead to an azimuthal asymmetry of the detected pseudo-scalar hadron around the direction of a transversely polarized quark. The Collins function describes the correlation between quark's transverse spin and the hadron's transverse momentum and can be regarded as a "quark polarimeter" for detecting the transverse spin of the fragmenting quark.

Beside being chirally-odd, the Collins function is also time-reversal odd, since it gives rise to a term proportional to $(\vec{k} \times \vec{p}_{h\perp}) \cdot \vec{s}_q$ in the quark fragmentation process (\vec{k} and \vec{s}_q are the momentum and the transverse spin of the fragmenting quark, and $\vec{p}_{h\perp}$ is the transverse momentum of the hadron). The existence of this novel T-odd fragmentation function requires interference of two amplitudes with different imaginary parts in the fragmentation process. Several recent model calculations⁶ for the fragmentation process have considered a pion-quark coupling tree-level diagram together with a pion or a gluon loop, and these calculations suggest a substantial magnitude for the Collins function. An interesting constraint on the Collins function has been obtained based on the conservation of transverse momentum during the parton fragmentation process⁷. This Schaefer-Teryaev sum rule shows that the moment of the Collins function vanishes when the function is summed over all hadron states. On the experimental side, a recent analysis⁸ of the $e^+e^- \rightarrow \pi\pi$ data from Belle has shown a significant azimuthal asymmetry attributed to the Collins function. Any new experimental information on the Collins function is of much interest not only for its connection to the extraction of δq in SIDIS, but also for understanding the nature of this novel T-odd fragmentation function.

An entirely different mechanism can also contribute to the azimuthal asymmetry in SIDIS. It was suggested by Sivers⁹ that correlations between the transverse spin of the target nucleon and the transverse momentum of the unpolarized quark could lead to single-spin asymmetries in various processes. This correlation is expressed in terms of the ‘‘Sivers Function’’, which is an example of transverse-momentum-dependent (TMD) parton distribution functions. An interesting feature of the Sivers function is that it is related to the forward scattering amplitude of $N \Rightarrow q \rightarrow N \Leftarrow q$ where the helicity of the target nucleon is flipped. This helicity flip of the nucleon must involve the orbital angular momentum of the unpolarized quark. Therefore, the Sivers function is connected to the quark’s orbital angular momentum.

As a time-reversal odd object, the Sivers function requires initial/final state interactions via a soft gluon. As shown recently^{10,11,12}, such interactions are incorporated in a natural fashion by the gauge link that is required for a gauge-invariant definition of the TMD parton distribution. A striking prediction¹¹, based on the time-reversal symmetry of QCD, is that the Sivers function as deduced from SIDIS will change sign in the Drell-Yan process. If confirmed by experiment, this would shed much light on the issue of universality for the TMD parton distributions. Several model calculations for the Sivers function have been carried out recently. Most of these calculations use the spectator model with scalar and axial-vector diquarks^{10,13,14,15,16}. A calculation based on the MIT bag model has also been performed¹⁷. Note that T-odd distribution functions vanish in chiral soliton model, where gluonic degrees of freedom are absent¹⁸. An unambiguous measurement of Sivers function would be very valuable for understanding the nature of the TMD parton distributions.

Several recent measurements at HERMES using longitudinally polarized hydrogen and deuterium targets have observed azimuthal asymmetries in SIDIS¹⁹. However, separation of the Collins from the Sivers mechanism is hindered by the fact that

both mechanisms have a common $\sin\phi_h$ azimuthal behavior. Moreover, subleading-twist effects could also have a large contribution. These difficulties are avoided when transversely polarized targets are used. The additional degree of freedom associated with the azimuthal angle ϕ_S of the target nucleon polarization direction allows an unambiguous separation of these two mechanisms, namely, a $\sin(\phi_h - \phi_S)$ dependence for the Sivers mechanism and a $\sin(\phi_h + \phi_S)$ distribution for the Collins mechanism²⁰.

Both the HERMES and the COMPASS experiments have recently reported first results from SIDIS data collected with transversely polarized targets. The HERMES experiment uses 27.6 GeV positron beam bombarding a transversely polarized hydrogen gas target. Scattered positrons were detected in coincidence with charged pions and the mean values of the kinematic parameters are $\langle x \rangle = 0.09$, $\langle y \rangle = 0.54$, $\langle Q^2 \rangle = 2.41 \text{ GeV}^2$, $\langle z \rangle = 0.36$, and $\langle P_{\pi\perp} \rangle = 0.41 \text{ GeV}/c$. In a recent HERMES publication²¹, signals for both the Collins and Sivers mechanisms were reported for data recorded in the 2002-2003 running period. Very recently, preliminary HERMES results based on nearly five times more statistics have been presented²². Fig. 1 shows the Collins and Sivers moments as a function of x , z and $P_{\pi\perp}$. The average Collins moment is positive for π^+ and negative for π^- . This behavior is expected if the transversity distributions resemble the helicity distribution such that δu is positive and δd is negative. It is quite surprising that the magnitude of the π^- moment is at least as large as that for π^+ , since one expects $|\delta u| > |\delta d|$ in analogy with $|\Delta u| > |\Delta d|$. This expectation is based on the assumption that the disfavored Collins fragmentation function is small compared with the favored one. The HERMES result suggests that this assumption might not be valid.

Figure 1 also shows that the Sivers moment is non-zero and positive for π^+ . This result provides the first evidence for a T-odd parton distribution function in SIDIS. With the sign convention²³ adopted by HERMES and the expectation that the π^+ moment is dominated by u quark, the positive Sivers moment for π^+ implies a negative value for the Sivers function for the u quark. Figure 1 shows that the Sivers moment for π^- is consistent with zero, in striking contrast to the π^+ result.

The COMPASS experiment has also reported²⁴ the first measurement of Collins and Sivers azimuthal asymmetries for 160 GeV/c muon beam incident on transversely polarized ^6LiD target. Figure 2 shows that both the Collins and the Sivers asymmetries are consistent with zero.

The striking pion-charge dependences of the Collins and Sivers moments observed by HERMES, as well as the remarkable difference between the HERMES and COMPASS results on proton and deuteron targets, suggest a strong and unexpected flavor dependence of both the Collins and Sivers functions. The HERMES and COMPASS data have been analyzed^{25,26,27} very recently to extract the Collins and Sivers functions. Using a parameterization of the Collins functions with the form:

$$H_1^{\perp f av}(z) = C_{fav} z(1-z) D_1^{fav}(z), \quad H_1^{\perp unf av}(z) = C_{unfav} z(1-z) D_1^{fav}(z), \quad (1)$$

and adopting a parameterization²⁸ of the transversity distribution based on satura-

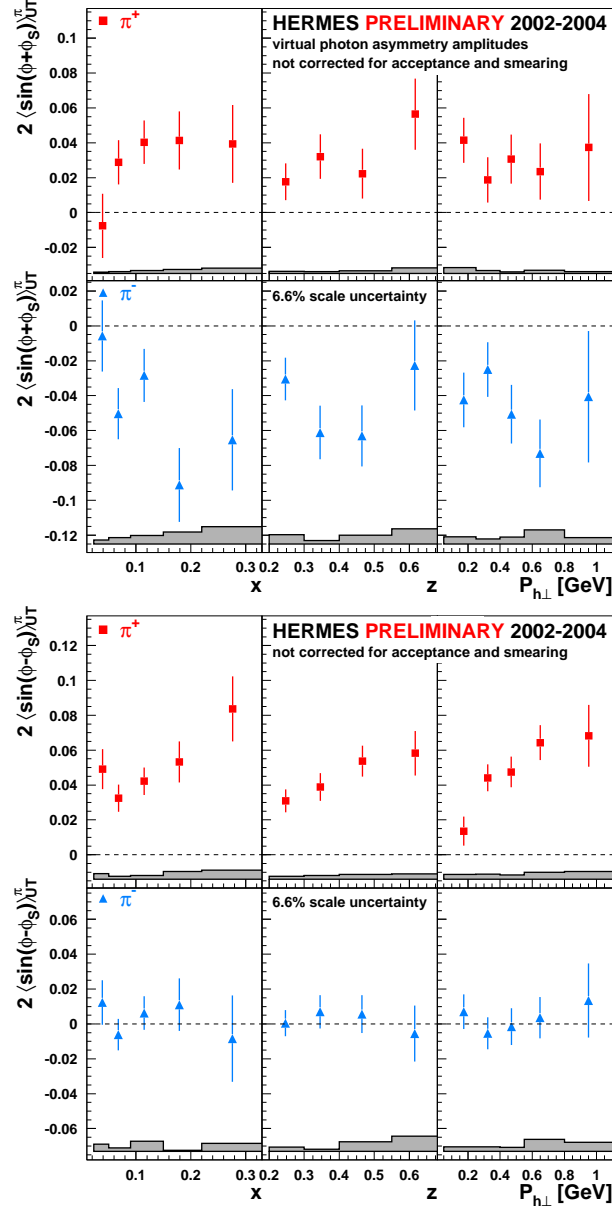


Figure 1: Collins and Sivers moments from the HERMES preliminary results on transversely polarized hydrogen data²².

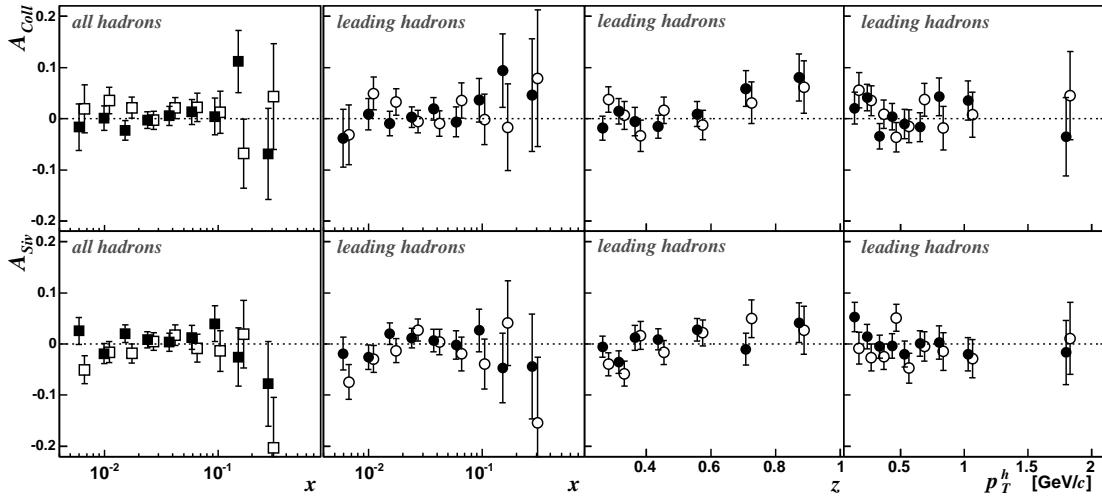


Figure 2: Collins asymmetry and Sivers asymmetry from COMPASS using a transversely polarized ${}^6\text{LiD}$ target²⁴.

tion of the Soffer inequality²⁹, the authors of ref.²⁵ fitted the HERMES data²² and obtained

$$C_{fav} = -0.29 \pm 0.04, \quad C_{unfav} = 0.33 \pm 0.04, \quad (2)$$

where the subscripts *fav* and *unfav* refer to the favored and unfavored fragmentation functions. The result that the unfavored Collins function is approximately equal to the favored one with opposite sign is actually consistent with an expectation based on a conjecture²⁵ motivated by the Schaefer-Teryaev sum rule. A description of Collins fragmentation function from string breaking³⁰ also gives opposite signs for the favored and unfavored function. It would be very important to test this interesting result with additional measurements. The authors of ref.²⁵ found that their calculations of the Collins asymmetries for deuteron target are consistent with the very small asymmetries observed by COMPASS. The small predicted Collins asymmetries are attributed to the partial cancellation between the proton and neutron contributions, as well as the presumably small sea-quark transversity distributions at small x region. A measurement of the Collins asymmetries at the valence-quark region using a transversely polarized ${}^3\text{He}$ target, as proposed in this proposal, would provide very valuable new inputs for understanding the difference between the HERMES and the COMPASS results.

Several analysis^{25,26,27,31} of the HERMES data for extracting the Sivers functions have all shown that d quark Sivers function is larger in magnitude than the u quark one, and with opposite sign, as shown in Fig. 3. This result reflects the striking difference of the Sivers asymmetries observed for π^+ and π^- . It is interesting that the signs of the u and d Sivers functions are consistent with the expectations in ref.³², where a connection of the quark's Sivers function to the quark's contribution to pro-

ton's anomalous magnetic moment is made. The vanishing Siverts moments found by COMPASS can be well reproduced by these authors. The smallness of the Siverts asymmetries is again attributed to the small- x kinematic region of COMPASS and the cancellation of contributions from proton and neutron in the target. The measurement proposed here would provide crucial new information for understanding the flavor structure of the Siverts function.

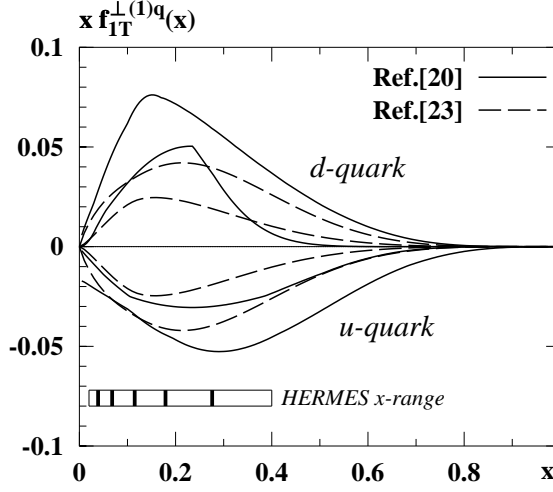


Figure 3: The first moment of the Siverts functions for u and d quarks extracted from fits³¹ to the HERMES data²².

2.1 Transverse target spin related SIDIS cross sections

The differential cross section in a SIDIS ($e, e'h$) reaction, in which the beam is not polarized and the target is transversely polarized, can be expressed at leading-twist as the sum of a target spin-independent and a target spin-dependent term:

$$\begin{aligned} \frac{d\sigma^h}{dx_B dy dz_h d\phi_h} &\equiv d\sigma^h = d\sigma_{UU} + d\sigma_{UT}, \\ &= d\sigma_{UU} + d\sigma_{UT}^{Collins} + d\sigma_{UT}^{Siverts} + d\sigma_{UT}^{others}. \end{aligned} \quad (3)$$

Each term in Eq. 3 can be expressed as convolutions of parton density and fragmentation functions³³:

$$d\sigma_{UU} = \frac{4\pi\alpha^2 s}{Q^4} (1 - y + \frac{y^2}{2}) \sum_q e_q^2 [f_1^q \otimes D_1^q], \quad (4)$$

$$d\sigma_{UT}^{Collins} = \frac{4\pi\alpha^2 s}{Q^4} |S_T| (1 - y) \sin(\phi_h + \phi_S) \sum_q e_q^2 [h_1^q \otimes H_1^{\perp q}], \quad (5)$$

$$d\sigma_{UT}^{Siverts} = \frac{4\pi\alpha^2 s}{Q^4} |S_T| (1 - y + \frac{y^2}{2}) \sin(\phi_h - \phi_S) \sum_q e_q^2 [f_{1T}^{\perp q} \otimes D_1^q], \quad (6)$$

$$d\sigma_{UT}^{others} = \frac{4\pi\alpha^2 s}{Q^4} |S_T| (1-y) \frac{P_{h\perp}^2}{6z^2 M_N^2} \sin(3\phi_h - \phi_S) \sum_q e_q^2 [h_{1T}^{\perp q} \otimes H_1^{\perp q}]. \quad (7)$$

The azimuthal angles are defined according to the Trento conventions²³ as shown in Fig. 4.

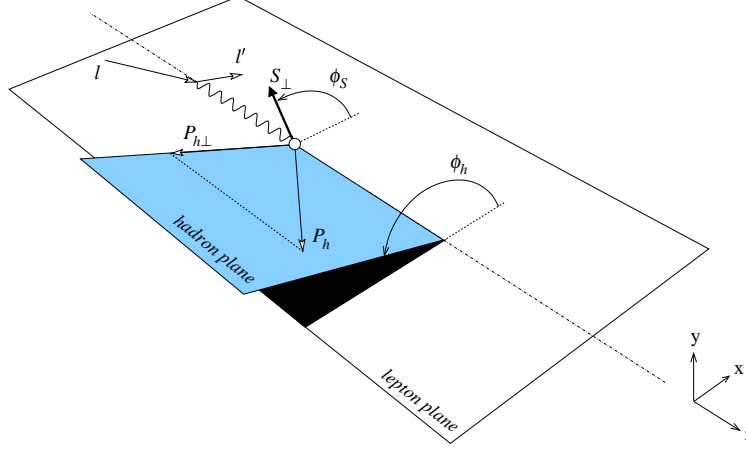


Figure 4: The definition of ϕ_h and ϕ_S according to the Trento conventions.

The convolution in Eq. 4-Eq. 5 represents an integration over transverse momentum of initial (\mathbf{k}_T) and final quark (\mathbf{p}_T) with proper weighting³³, i.e.

$$[.. \otimes ..] = \int d^2 \mathbf{p}_T d^2 \mathbf{k}_T \delta^{(2)}(\mathbf{p}_T - \frac{\mathbf{P}_{h\perp}}{z} - \mathbf{k}_T)[...]. \quad (8)$$

These convolutions can be reduced to simple products if the $|P_{h\perp}|$ -weighted integrations cover to infinite $|P_{h\perp}|$ or explicit \mathbf{p}_T and \mathbf{k}_T dependencies (like Gaussian distributions) are introduced.

2.2 Transverse target single-spin asymmetry

Neglecting the $3\phi_h$ term, which is expected to be small by most model calculations, the target SSA can be defined as:

$$A_{UT} \equiv \frac{1}{|S_T|} \frac{d\sigma_{UT}}{d\sigma_{UU}} = \frac{1}{|S_T|} \frac{d\sigma(\phi_h, \phi_S) - d\sigma(\phi_h, \phi_S + \pi)}{d\sigma(\phi_h, \phi_S) + d\sigma(\phi_h, \phi_S + \pi)}. \quad (9)$$

The Collins and Sivers asymmetry have different angular dependences:

$$A_{UT}(\phi_h, \phi_S) = A_{UT}^{Collins} \sin(\phi_h + \phi_S) + A_{UT}^{Sivers} \sin(\phi_h - \phi_S). \quad (10)$$

The HERMES^{21,22} and the COMPASS²⁴ paper used the notation of moments $2\langle \sin(\phi_h + \phi_S) \rangle_{UT}$ and $2\langle \sin(\phi_h - \phi_S) \rangle_{UT}$, which are corresponding to:

$$A_{UT}^{Collins} \equiv 2\langle \sin(\phi_h + \phi_S) \rangle_{UT} \cdot D_{nn}, \quad (11)$$

$$A_{UT}^{Sivers} \equiv 2\langle \sin(\phi_h - \phi_S) \rangle_{UT} \quad (12)$$

where $D_{nn} \equiv (1-y)/(1-y+\frac{y^2}{2})$ for COMPASS. The definition of HERMES includes the longitudinal virtual photon effect $R = \sigma_L/\sigma_T$ to replace D_{nn} with $B(y)/A(x, y)$ where $B(y) = (1-y)$, and $A(x, y) = \frac{y^2}{2} + (1-y)\frac{1+R(x,y)}{1+Q^2/\nu^2}$. For this experiment, the differences between D_{nn} and $B(y)/A(x, y)$ are rather small, at a few percent level.

From Eq. 4-5 we have:

$$A_{UT}^{Collins} \equiv D_{nn} 2\langle \sin(\phi_h + \phi_S) \rangle_{UT} = D_{nn} \cdot \frac{\sum_q e_q^2 [h_1^q \otimes H_1^{\perp q}]}{\sum_q e_q^2 [f_1^q \otimes D_1^q]}, \quad (13)$$

$$A_{UT}^{Sivers} \equiv 2\langle \sin(\phi_h - \phi_S) \rangle_{UT} = \frac{\sum_q e_q^2 [f_{1T}^{\perp q} \otimes D_1^q]}{\sum_q e_q^2 [f_1^q \otimes D_1^q]}. \quad (14)$$

Although Eq. 13 and Eq. 14 are defined without any ambiguity, different experiments usually cover different ranges in the convolution of Eq. 8 due to finite P_\perp^h coverages, making it very difficult or impossible for a direct comparison between A_{UT} results from different experiments. Only after explicit \mathbf{p}_T and \mathbf{k}_T dependencies are introduced is such a comparison meaningful. For an ideal experiment with infinite P_\perp coverage, SSA asymmetries can be weighted by $|P_\perp^h/z_h M_h|$, such that the convolutions in Eq. 8 reduce to products:

$$A_{UT}^{Collins} = \frac{(1-y)}{(1-y+\frac{y^2}{2})} \frac{\sum_q e_q^2 h_1^q(x) \cdot H_1^{\perp(1)q}(z)}{\sum_q e_q^2 f_1^q(x) \cdot D_1^q(z)}, \quad (15)$$

$$A_{UT}^{Sivers} = \frac{\sum_q e_q^2 f_{1T}^{\perp(1)q}(x) \cdot D_1^q(z)}{\sum_q e_q^2 f_1^q(x) \cdot D_1^q(z)}. \quad (16)$$

2.3 Factorization in SIDIS and recent JLab data

Recently, QCD factorization in SIDIS has been proved by Ji, Ma and Yuan explicitly³⁴ in the case of hadrons emitted in the current fragmentation region with low transverse momentum $P_{\perp h} \ll Q$. QCD factorization of spin-dependent cross sections in SIDIS has also been proved for the low $P_{\perp h}$ case³⁵. Most importantly, recent JLab data have shown that even the leading order x - z factorization assumption, under which the parton densities (x -dependent) and the fragmentation functions (z -dependent) are factorized, works reasonably well at JLab energies.

In Fig. 5, preliminary SIDIS cross sections from Hall C E00-108 in $p(e, e'\pi^-)$ and $p(e, e'\pi^+)$ reactions³⁶ at $x = 0.3$ are shown to agree with a SIDIS Monte Carlo simulation which assumed x - z factorization. This agreement indicates that information on the quark distributions is well-preserved in SIDIS reactions at JLab energies. The lack of any resonance structures at $z < 0.70$ ($W' > 1.5$ GeV) indicates that the contributions from exclusive resonance production are not large when $W' > M_\Delta$, confirming earlier observations of Cornell experiments^{37,38} at $E_0 = 11$ GeV.

The existing double-spin asymmetry data³⁹ also suggest leading order x - z factorization at 6 GeV. Clear agreement of $A_{1p}^{\pi^+}$ between HERMES and CLAS data indicates the strong domination of current-quark fragmentation at JLab energy.

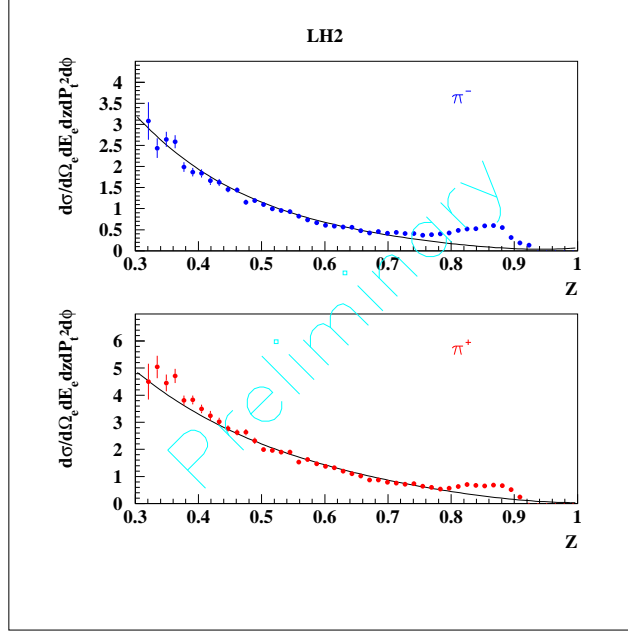


Figure 5: Preliminary SIDIS cross sections from Hall C E00-108. The cross sections in $p(e, e'\pi^-)$ and $p(e, e'\pi^+)$ at $x = 0.3$ are shown to agree with a SIDIS Monte Carlo simulation which assumed x - z factorization (solid line).

3 The Proposed Measurement

3.1 Overview

We plan to study the target single spin asymmetry (SSA) in the semi-inclusive deep-inelastic $n^\uparrow(e, e'\pi^-)X$ reaction on a transversely polarized ^3He target in Hall A with a 6 GeV beam. $(e, e'K^-)$ events will be treated as by-products. The average beam current will be $\approx 15 \mu\text{A}$. Although a polarized beam is not required to perform the SSA measurements, we request an 80% polarized electron beam for parasitic double-spin asymmetry measurements. Analysis of SSA will sum over the two beam helicities.

The experiment will use the Hall A left side high resolution spectrometer (HRS_L) at 16° as the hadron arm, and use the BigBite spectrometer at 30° beam-right as the electron arm. The BigBite detector configuration will be exactly the same as in Hall A G_E^n experiment⁴⁰ (E02013), which is scheduled to take production data in early 2006. The drift distance to the BigBite dipole magnet will be 1.50 m, instead of the 1.10 m in E02013. Since this experiment is a coincidence experiment with the HRS_L at a relatively low rate, the HRS spectrometer can be used for interaction vertex reconstruction such that most of the complications associated with the BigBite wire chamber track reconstruction can be eliminated, in contrast to the case of the G_{En} experiment. In addition, when a tight coincidence timing cut is further required we expect that the majority of the background tracks and random hits in the BigBite wire chambers can be easily eliminated.

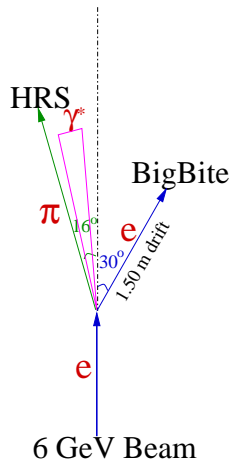


Figure 6: Experiment arrangement.

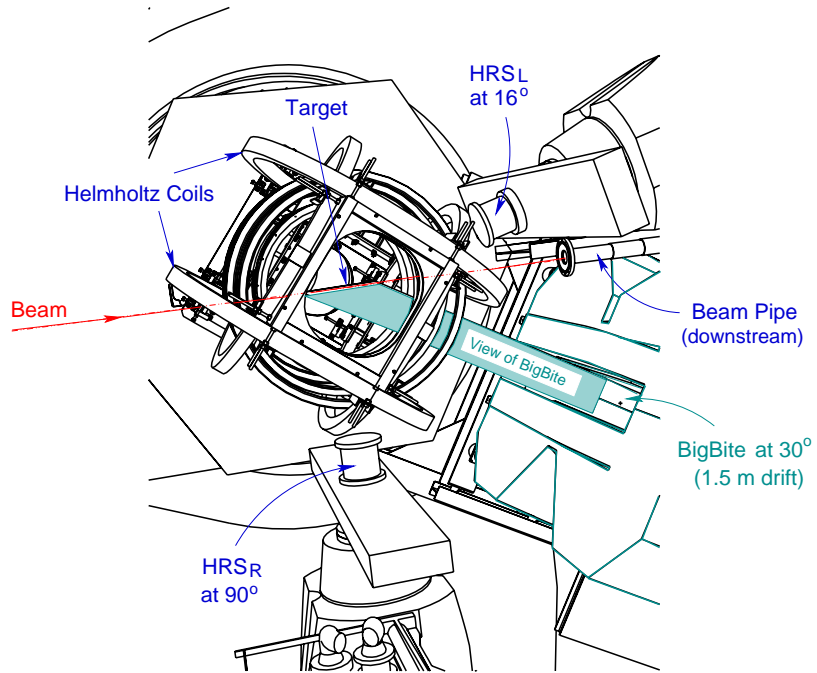


Figure 7: A top view near the pivot. The left HRS is shown at 16°, the BigBite dipole magnet is shown at 30° beam right and at a 1.5 meter drift distance. The right HRS is at 90° as a luminosity monitor. The target coils are arranged to avoid interference with the beam line and the spectrometers.

The Hall A high luminosity polarized ^3He target will be used with a 40 cm long cell. The Helmholtz coils and laser optics need to be modified to provide a target polarization along two specific orientations: the vertical direction and transverse in-plane relative to the beam direction. The experimental arrangement is illustrated in Fig. 6 and a close-up view near the pivot is shown in Fig. 7.

3.2 The choice of kinematics

The definitions of the kinematic variables are the following: Bjorken- x , which indicates the fractional momentum carried by the struck quark, is $x = Q^2/(2\nu M_N)$, where M_N is the nucleon mass. The momentum of the outgoing hadron is p_h and the fraction of the virtual photon energy carried by the hadron is: $z = E_h/\nu$. W is the invariant mass of the whole hadronic system and W' is the invariant mass of the hadronic system without the detected hadron. We have:

$$W^2 = M_N^2 + Q^2\left(\frac{1}{x} - 1\right),$$

$$W'^2 = (M_N + \nu - E_\pi)^2 - |\vec{q} - \vec{p}_\pi|^2. \quad (17)$$

We chose to cover the highest possible W with a 6 GeV beam, $2.33 < W < 3.05$ GeV, corresponds to $0.135 < x < 0.405$ and $1.31 < Q^2 < 3.10$ (GeV/c) 2 . We also chose to detect the leading fragmentation pion which carries $z \approx 0.5$ of the energy transfer to favor current fragmentation. The value of W' is also chosen to be as high as possible with a cut of $W' > 1.5$ GeV to avoid contributions from resonance production channels. The kinematics for each x -bin center are listed in Table 1. Because of the large momentum bite of the BigBite spectrometer, only one BigBite setting is needed to cover all the kinematics listed in Table 1. Only one hadron arm momentum setting, $p_\pi = 2.4$ GeV/c will be taken. The corresponding values of W' and z are listed in Table 1.

Table 1: Nominal kinematics of each x -bin center for beam energy of $E = 6.0$ GeV. One BigBite setting will cover all the kinematics listed. E' and θ_e are the electron arm momentum and angle. θ_q indicates the direction of \vec{q} . The hadron arm angle is fixed at 16° .

E' GeV	θ_e deg.	$\langle x \rangle$	W GeV	Q^2 GeV 2	θ_q deg.	z_π	p_π GeV/c	W' GeV
						$\theta_\pi = 16.0^\circ$		
0.815	30.0	0.135	3.050	1.310	4.40	0.46	2.40	2.20
1.246	30.0	0.225	2.793	2.003	7.22	0.51	2.40	1.99
1.612	30.0	0.315	2.554	2.592	9.93	0.55	2.40	1.80
1.925	30.0	0.405	2.331	3.095	12.52	0.59	2.40	1.62

3.3 Phase spaces, Collins angle and Sivers angle coverage

The phase space coverage is obtained from a detailed Monte Carlo simulation which includes realistic spectrometer models as well as target and detector geometry. The coverage in the (Q^2, x) and (W, x) planes is shown in Fig. 8, and the coverage in the (W', x) and (P_\perp, x) planes is shown in Fig. 9, color coded for each x -bin.

The angular coverage of ϕ_h^l and ϕ_S^l is shown in Fig. 10 and Fig. 11. Four settings of target spin orientation will be taken with $\langle \phi_S^l \rangle = 0^\circ, 90^\circ, 180^\circ$ and 270° . For every x -bin in this experiment, the full 2π range of the Collins angle is covered. Collins angle coverage is shown in Fig. 12. Sivers angle coverage is shown in Fig. 13.

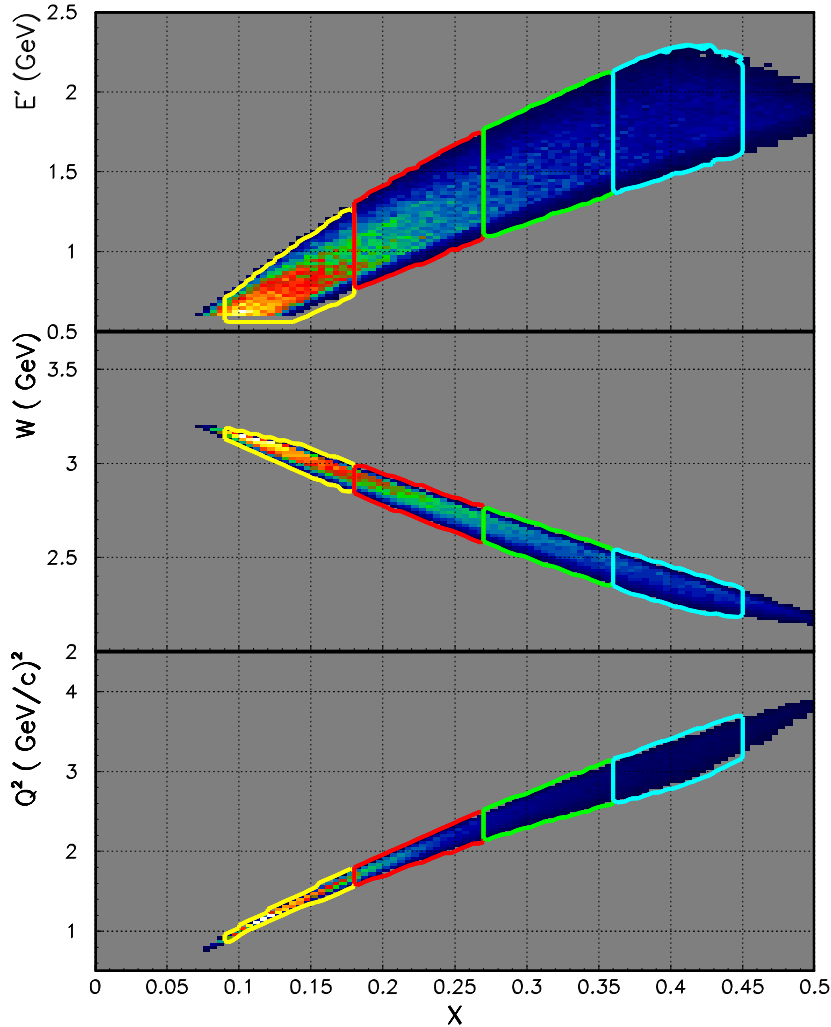


Figure 8: Available phase space in the (Q^2, x) and (W, x) planes with each x -bin in different colors.

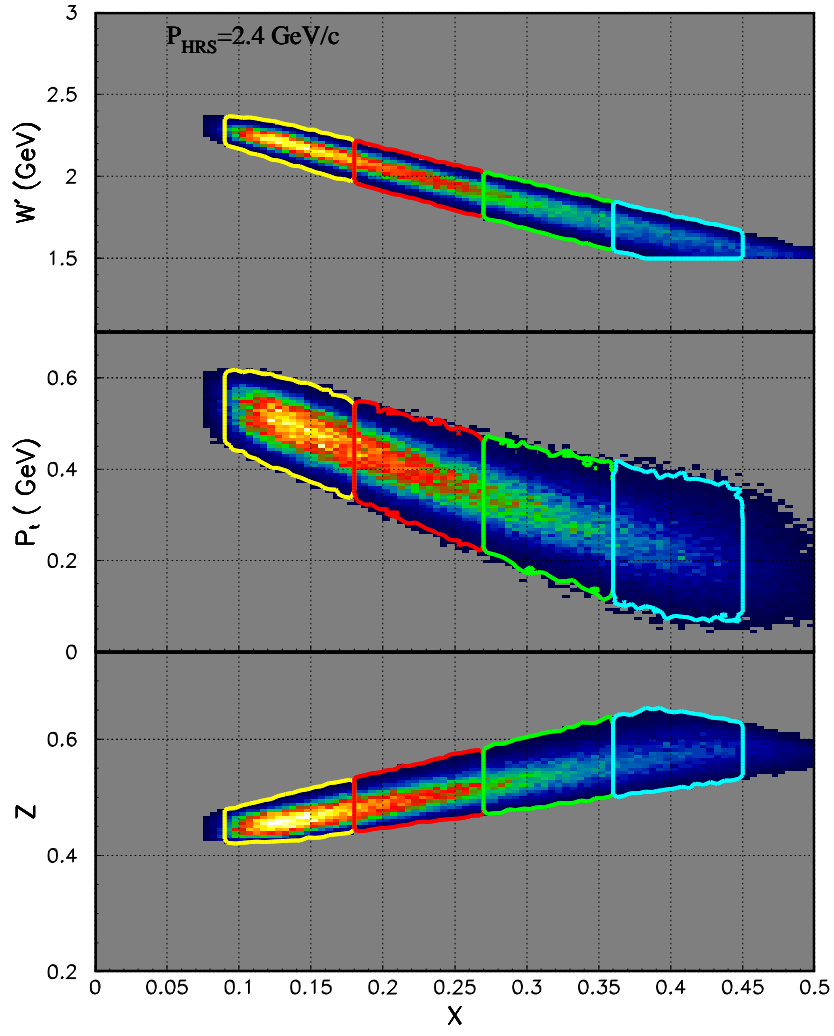


Figure 9: Same as in Fig. 8, phase space coverage in (W', x) , (P_\perp, x) and (z_π, x)

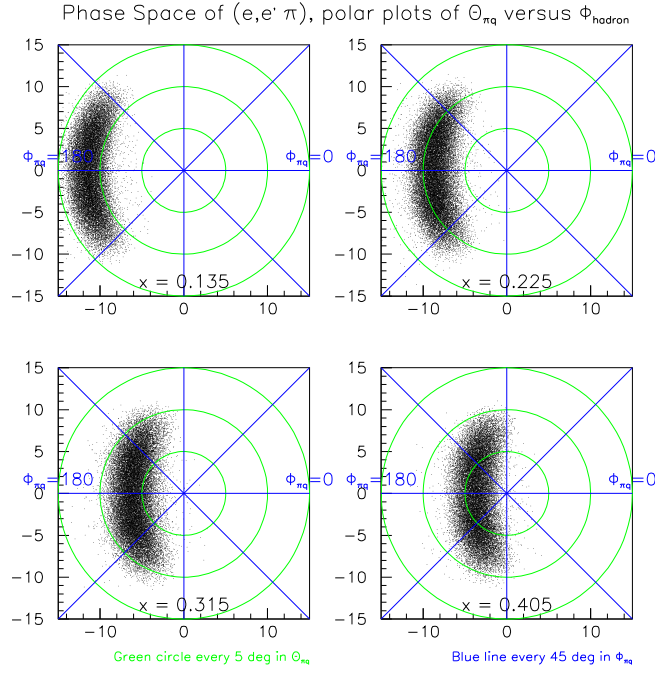


Figure 10: Angular coverage of ϕ_h^l are shown for each x -bin, viewed along \vec{q} .

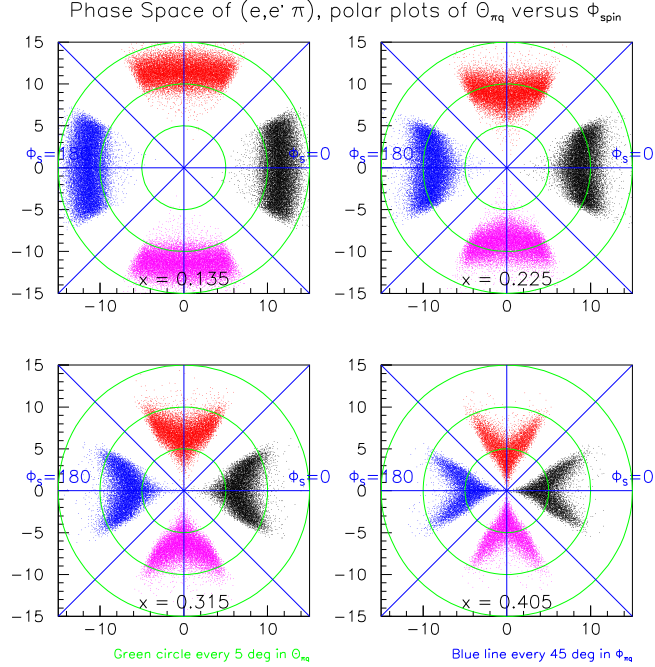


Figure 11: Angular coverage of ϕ_S^l are shown for each x -bin, viewed along beam. Black: $\phi_S^l = 0^\circ$. red: $\phi_S^l = 90^\circ$, blue: $\phi_S^l = 180^\circ$, purple: $\phi_S^l = 270^\circ$.

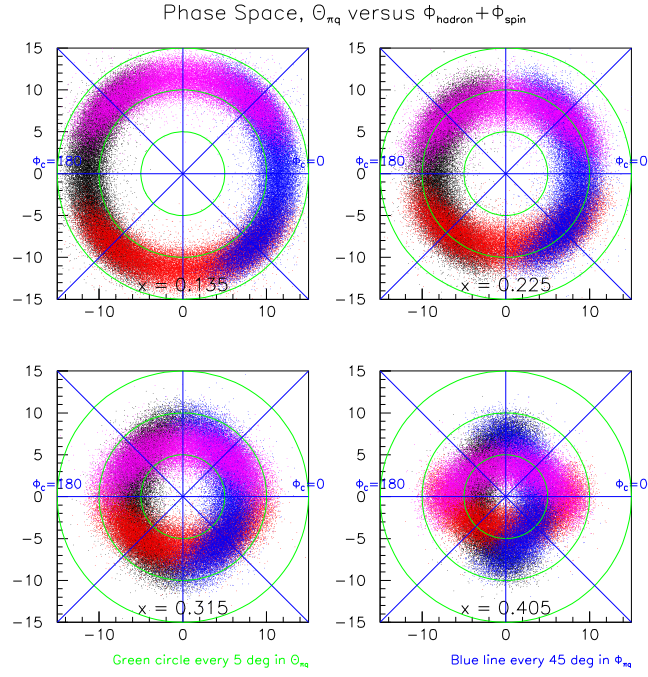


Figure 12: Collins angle coverage of $\phi_{Collins} = \phi_h^l + \phi_S^l$ are shown for each x -bin. Black: $\phi_S^l = 0^\circ$. red: $\phi_S^l = 90^\circ$, blue: $\phi_S^l = 180^\circ$, purple: $\phi_S^l = 270^\circ$. For every x -bin in this experiment, the full 2π range of the Collins angle is covered.

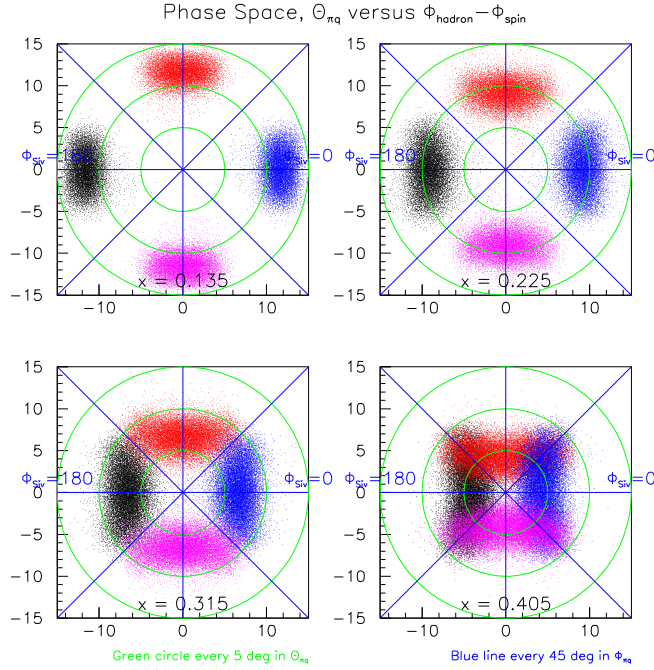


Figure 13: Sivers angle coverage of $\phi_{Sivers} = \phi_h^l - \phi_S^l$ are shown for each x -bin. Black: $\phi_S^l = 0^\circ$. red: $\phi_S^l = 90^\circ$, blue: $\phi_S^l = 180^\circ$, purple: $\phi_S^l = 270^\circ$.

3.4 The experimental observable

The target single spin asymmetry $A_{UT}^h(\phi_h, \phi_S)$ can be obtained directly from the luminosity-normalized yield:

$$A_{UT}^h(\phi_h, \phi_S) = \frac{1}{P_T} \cdot \frac{N(\phi_h, \phi_S) - N(\phi_h, \phi_S + \pi)}{N(\phi_h, \phi_S) + N(\phi_h, \phi_S + \pi)} \quad (18)$$

The relative luminosity will be monitored by various spectrometer singles rates and the downstream luminosity monitors. In addition, frequent target spin-flips, once every 10-20 minutes, are expected to further reduce the uncertainties of the luminosity ratio.

3.5 The electron arm: BigBite

The BigBite spectrometer will be located at 30° and at a drift distance of 1.50 m, instead of the 1.1 m drift in E02013. The BigBite detector package will be identical to what will be used in the G_E^n experiment (E02013). Three sets of wire chambers will be used to provide tracking information followed by a pre-shower, scintillator and shower assembly to provide trigger and particle ID for the electrons. The BigBite dipole magnet will be set at the full current with $|\vec{B}| = 1.2$ T. Charged particles originated from the target with momentum less than 0.2 GeV/c will not reach the detectors, as shown in Fig. 14.

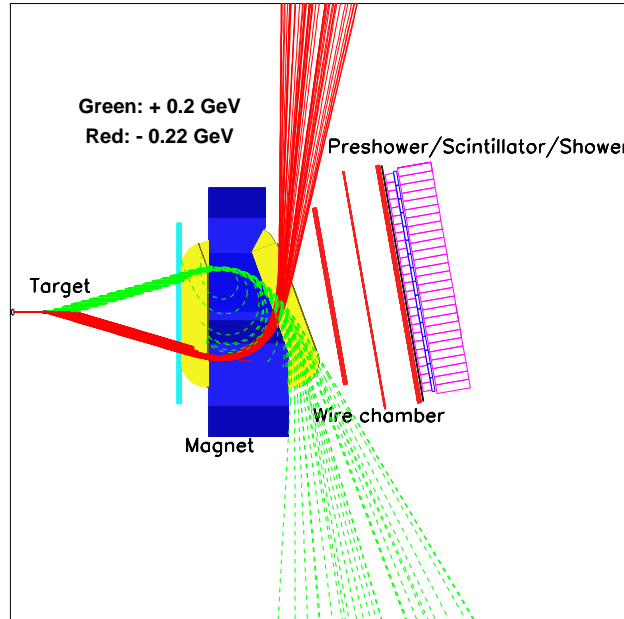


Figure 14: Charged particle trajectories through the BigBite magnet. Positive particles with momentum less than 200 MeV/c and negative particles with momentum less than 220 MeV/c will not reach the detectors. The location of wire chambers, pre-shower, trigger scintillator planes and shower lead glass arrays are also indicated.

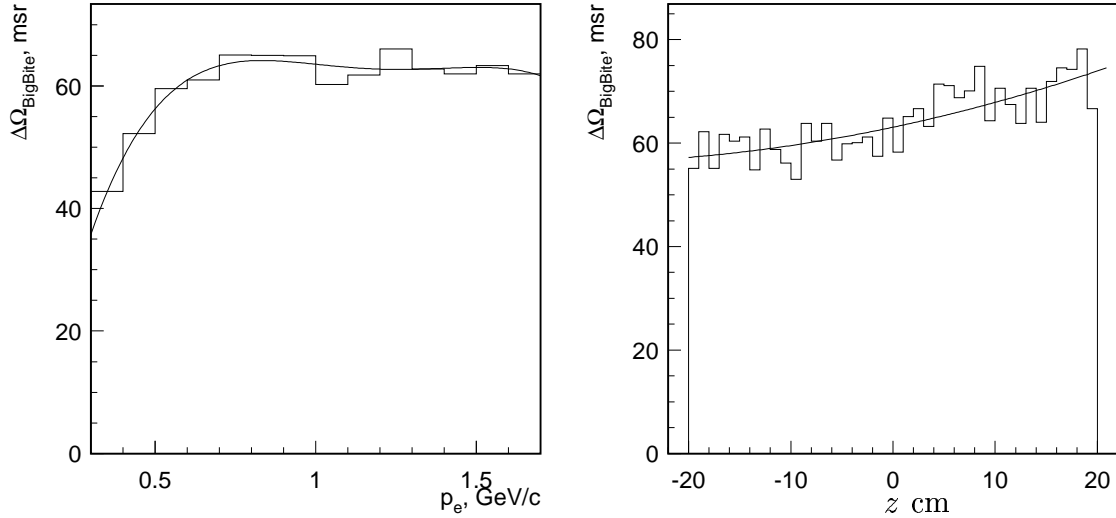


Figure 15: BigBite acceptance as a function of particle momentum (left) and as a function of interaction point (right).

The BigBite collaboration has already built three sets of wire chambers, each with U-U', V-V' and X-X' planes. The sense wire separation is 2.0 cm, corresponding to a drift cell size of 1.0 cm and a maximum drift time of 100 ns. A GEANT-3 Monte Carlo simulation⁴⁰ has shown that with a typical chamber resolution of 200 μm , the momentum resolution ($\delta p/p$) is $\approx 2\%$. The angular resolution is 3.0 mrad in each direction, causing a few MeV uncertainty in P_\perp reconstruction. The vertex resolution (at 30°) will be better than 2.0 cm along the beam. Since this experiment does not seek to resolve any structure in the final states, and the SIDIS events will be grouped in rather large x -bins, the momentum and angular resolutions designed for E02-013 will be adequate for this experiment.

The electron particle identification (PID) will be provided by a set of pre-shower and shower detectors. The pre-shower blocks are made of TF-5 lead glass, $10 \times 10 \times 37 \text{ cm}^3$ each, covering an active area of $210 \times 74 \text{ cm}^2$, with 10 cm (3 r.l.) along the particle's direction. The total absorption shower blocks are made of TF-2 lead glass, $8.5 \times 8.5 \times 34 \text{ cm}^3$ each, covering an active area of $221 \times 85 \text{ cm}^2$, with 34 cm (13 r.l.) along the particle's direction. The total depth of lead glass is enough to contain electron showers with energies up to 10 GeV, with an energy resolution of $8.0\%/\sqrt{E}$. A typical pion rejection factor of 100:1 is expected from offline cuts that combines pre-shower and shower information. Based on Hall C SOS spectrometer data taken at a similar kinematics, the expected worst case singles π^-/e^- ratio in BigBite will be no more than 100:1 for this experiment. Since we are only interested in coincidence events in this experiment, a cut of coincidence TOF and a cut of two-particle vertex consistency will reduce the random π^- contamination to a negligible

level (see Table 5).

The BigBite acceptance as a function of particle momentum and interaction point is shown in Fig. 15. An average solid angle of 64 msr is expected, with the vertical angle $\Delta\theta_t = \pm 240$ mrad ($\pm 13.7^\circ$) and the horizontal angle $\Delta\phi_t = \pm 67$ mrad ($\pm 3.8^\circ$).

Single particle background, BigBite single arm trigger and track reconstruction

The background rates in the BigBite detectors are calculated using the Monte Carlo simulation code GDINR⁴¹. For particles with momentum above 200 MeV/c, the integrated electron rate is less than 65 kHz, π^- rate is 380 kHz, π^+ rate is 500 kHz and the positron rate is 20 kHz. The majority of the charged particle background comes from low energy protons with $p > 200$ MeV/c ($T_p > 21$ MeV) at a rate of 2.0 MHz, comparable to the situation of E02-013. The majority of these protons will be stopped by the pre-shower detector and never reach the trigger scintillators. The BigBite single-arm trigger will be formed from a logical AND of a scintillator hit and an energy deposition of at least 200 MeV in the pre-shower or in the shower detectors. Only a small fraction of charged pions are expected to deposit enough energy in pre-shower and shower to generate such a trigger. The raw BigBite single-arm trigger rate is expected to be less than 200 kHz.

The low energy particle background on BigBite wire chambers is the major concern of this experiment. An extensive Monte Carlo background simulation has been carried out, and has been cross checked with rate information from several test runs. More details of the simulation are attached in Appendix-II. According to the simulation, the wire chamber rate will be at the level of 10-20 MHz per chamber, similar to the situation in the G_E^n experiment (E02-013). Recently, drift chambers of a similar design have performed well during the Hall C hyper-nuclear experiment at a comparable background rate.

By taking the BigBite magnet to a 1.5 meter drift distance, extra space is available before the magnet and between the detectors and the downstream beam pipe to construct shielding and to install collimators. A steel plate of 2 inch thickness on the downstream side, for example, can reduce the wire chamber activity by a factor of ten. The effectiveness of side shielding is illustrated in a GEANT simulation as shown in Fig. 16. We expect that by the time G_E^n (E02-013) starts taking production data in February 2006, shielding improvements of BigBite will make the background level acceptable to both the G_E^n experiment and this experiment.

Since the drift time window is 100 ns, the average multiplicity will be $1 \sim 2$ hits/plane for each trigger. This type of chamber background activity could result in several candidate tracks for a single arm experiment, or for an $(e, e'n)$ type measurement, such as in E02-013. For two-charge particle coincidence measurement, such as this experiment, in which the trigger involves the timing coincidence from two spectrometers, the on-line trigger will be rather clean, especially when the HRS_L singles trigger has a relatively low rate. In addition, high resolution vertex infor-

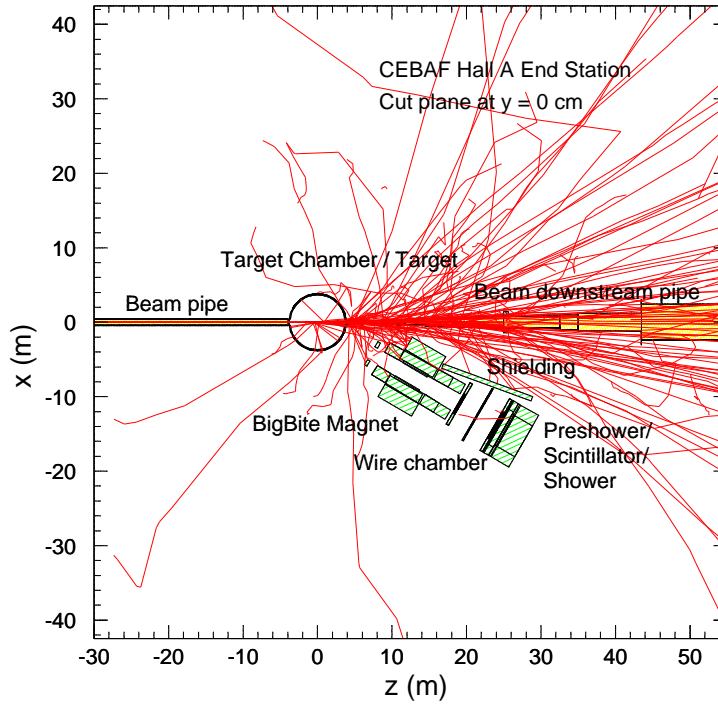


Figure 16: An illustration of the BigBite detector shielding plan. Most of the low-energy background particles can be shielded from hitting the wire chambers by a 2 inch steal plates on the downstream side.

mation from HRS_L on a long target helps in reducing the offline tracking ambiguity in BigBite, especially when the reconstruction on the HRS_L side is very clean. For BigBite tracking, the correct hit on the third chamber will be chosen closest to the center of the maximum shower in lead glass blocks. Since the BigBite dipole magnet does not cause much bending in the transverse direction, a straight line between the HRS_L reconstructed vertex and the center of the maximum shower at the calorimeter serves as the starting point of track reconstruction. In the dispersive direction, the location of the maximum shower cluster helps in track selection. Furthermore, the reconstructed particle momentum has to be consistent with the energy deposited in the calorimeter.

The G_E^n collaboration is planning an extensive optics calibration data taking during the BigBite commissioning in February, 2006. This set of optics data will also be used for the transversity experiment, after corrections in alignments and in differences of drift distance. Data taken during the E02-013 experiment will help to improve our BigBite magnet model, such that the acceptance will be well-understood, to better than $\pm 5\%$ level in the central region of the BigBite spectrometer. Although this experiment is designed to measure target spin correlated asymmetries, we expect that reasonable accuracies can also be reached for cross section ratios ($\pm 3\%$), spin-dependent and spin-independent multiplicities ($\pm 3\%$) and absolute cross sections ($\pm 5\text{--}8\%$).

3.6 The hadron arm HRS_L and hadron PID

The Hall A left-arm high resolution spectrometer (HRS_L) has been used in many experiments which require good particle identifications and accurate knowledge of acceptance ($\pm 3\%$). Absolute cross sections on polarized ^3He targets have been measured to the $\pm 5\%$ level in experiment E94-010 at a similar spectrometer angle.

This experiment will use a HRS_L detector package similar to the configurations in the Penta-quark search and in the Hyper-nuclear experiments. Since the expected e^-/π^- ratio is about 1:7, the existing two-layers of lead-glass blocks in HRS_L will be good enough to reject electrons. Two independent methods will be used for π^-/K^- separation: first, by a set of two threshold aerogel Cherenkov counters, and second, by a ring imaging Cherenkov detector (RICH). A third independent method, separation based on differences in coincidence time-of-flight, will serve as a cross check. At a momentum of 2.4 GeV/c, charged pions will fire both aerogel Cherenkov, A1 ($n=1.015$) and A2 ($n=1.055$), while charged Kaons will only fire A2.

The expected HRS_L singles rates are listed in Table. 2. The single-arm HRS_L trigger rate will be about 1.2 kHz, dominated by π^- , with an e^-/π^- ratio of 1:7. Through the path of 25 meters in HRS_L , the time-of-flight for different charged particles at $p = 2.4$ GeV/c are listed in Table 3. Assuming a TOF resolution of $\sigma = 0.85$ ns, π^-/K^- TOF separation will be at 2σ .

Table 2: Single arm rates in HRS_L.

P'(GeV/c)	Rate in Hz on HRS _L		
	π^-	K^-	e^-
2.4	1006	46	165

Table 3: TOF and Δ_{TOF} (relative to near light-speed e^\pm) for the relevant kinematics, and number of sigma separation (assuming a coincidence TOF resolution of 850 ps)

	HRS $p = 2.40$ GeV/c		
	e^-	π^-	K^-
TOF (ns)	83.39	83.53	85.14
Δ_{TOF}	0.00	0.14	1.75
N_σ		0.17	2.05

The left-arm RICH detector

The left-arm RICH detector⁴² was designed to optimally separate 2 GeV kaons from pions (and protons). The detector consists of a Freon (C₆F₁₄) radiator with a refractive index $n = 1.28$ followed by a proximity gap of 10 cm and a multi-wire/pad proportional chamber. The 11520 pads are read out by a multiplexed Sample&Hold electronics, with a VME based ADCs. The RICH operated successfully in 2004 and 2005 for the hyper-nuclear experiment E94-107, providing a Cherenkov angular resolution of 5 mrad ($\theta_\pi - \theta_K = 6\sigma_{\theta_\pi}$) corresponding to a pion rejection factor greater than 1000 at 95% efficiency (see table 4).

At a momentum of 2.4 GeV/c, the RICH will be able to separate π^-/K^- to $4.0 \sigma_{\theta_\pi}$ with a pion rejection factor of 120, suitable for this experiment. However, minor upgrades of the present RICH can be made at a modest cost to improve the separation to $5.7 \sigma_{\theta_\pi}$ corresponding to a pion rejection factor of 1000. These improvements include adding a stainless steel frame spacer to increase the proximity gap to 15.5 cm, and replacing the present radiator with a different kind of freon (C₅F₁₂ $n=1.24$). The cost of these upgrades is estimated to be \$15-20k. INFN-ROME group will take the technical responsibility of the RICH upgrade.

A GEANT3 based Monte Carlo has been developed to investigate the performance of the upgraded RICH. The results are summarized in Table 4 and shown in Fig. 17 for the present and the upgraded RICH.

An option of a pressurized gas Cherenkov vs. RICH

The Hall A Penta-quark experiment⁴³ is investigating the option of a pressurized gas Cherenkov in HRS_L. This option calls for a pressurized C₄F₁₀ gas at about 1.6 Atm ($n = 1.0025$). Charged pions at 2.4 GeV/c generate on average 12 photo-electrons while charged kaons are below the threshold. A combination of the pressurized gas Cherenkov with aerogel A1 and A2 will provide a π^-/K^- separation with proper

Table 4: The performance of the RICH for the present configuration and the configuration after the upgrade.

RICH Configuration	Momentum [GeV/c]	σ_{θ_π} [mrad]	$\theta_\pi - \theta_K$ [σ_{θ_π}]	π Rejection at 95% efficiency
Existing	2	5	6	> 1000
Existing	2.4	4.8	4	120
Upgraded:				
C ₅ F ₁₂ Gap = 15.5 cm	2.4	4.2	5.7	> 1000

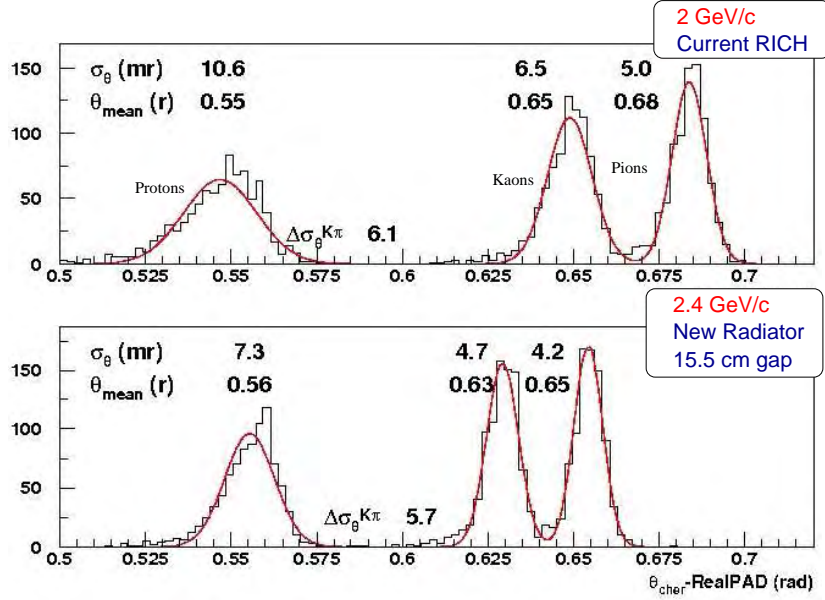


Figure 17: Monte Carlo simulation of the RICH performance: reconstructed Cherenkov angle for equally populated p , K^\pm and π^\pm samples. Top: the existing RICH at 2 GeV/c (normalized to the measured values); bottom: projected performance at 2.4 GeV/c after the radiator and proximity gap upgrade.

Table 5: Expected accidental rates

Selection	Rate [Hz]	Mode
Coincidence Window (50 ns)	10-20	Online
AND PreShower + Shower (BB and HRS)	1-2	Online
AND PreShower + Shower (BB and HRS)	0.1	Offline
AND Under the coincidence TOF peak	1.0×10^{-2}	Offline
AND Vertex Consistency	1.0×10^{-3}	Offline

redundancy for this experiment. Although the design details are not finalized yet, the estimated cost is at \$50k.

Since the RICH detector has proved good performances during E94-107 experiment and its upgrade is reasonably simple and inexpensive, we prefer the RICH detector as our first option. Positively identified charge kaons in SIDIS or exclusive kaon production channels could yield unexpected target single-spin asymmetries, as valuable by-products of this experiment.

3.7 Trigger and offline event selection

A coincidence time window of 50 ns will be enough to form the coincidence trigger. Trajectory corrected time-of-flight resolution is expected to be better than 2 ns. The raw accidental coincidence rate will be at 10-20 Hz. After the BigBite calorimeter ADC cut and the HRS_L PID cut, accidental coincidence events are not expected to survive at any significant level. Two-arm vertex consistency cut is expected to further eliminate the accidental events by an extra factor of 10, if there are any left. The true ($e, e'\pi^-$) coincidence rate is expected to be at 0.5-1.0 Hz level. The above values are summarized in Table 5

3.8 Luminosity monitors

The HAPPEX experiments E99-115 and E00-114 have recently completed an extended run. These experiments built 8 luminosity monitors called the Lumis. Each detector is made of Quartz with an air light guide. The monitors are placed downstream of the target within the beam pipe at a scattering angle of 7 mrad, see Fig. 18. The Lumis have performed very well during HAPPEX, monitoring the Luminosity to a very high precision of the 30 Hz beam helicity flips.

For this experiment, target spin will be flipped in a time period of ten to twenty minutes. To study the systematic effects of the Lumis in this time window, the data HAPPEX slug 30 was examined. This slug consisted of fourteen runs, each of 56 minutes in length. The data for each run was divided into four equal length time periods. The results from all eight Lumis were summed to remove Physics effects. Each sum was divided by the value from the Hall A beam charge monitor (BCM) to cancel beam jitter. The average result was determined for each 14 minute sequence.

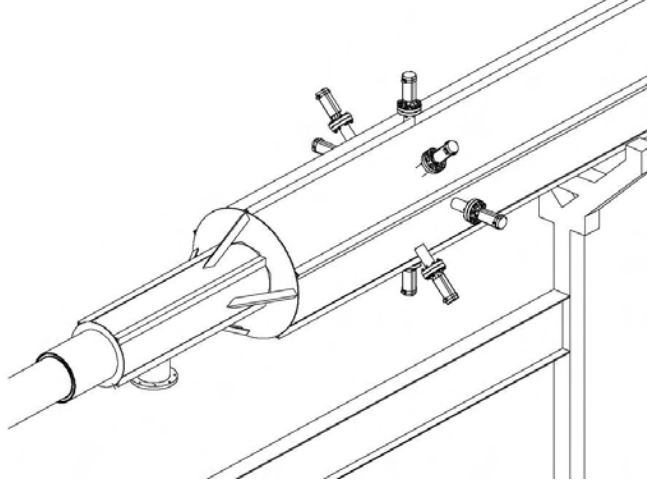


Figure 18: The Hall A Lumis in the beam pipe downstream of the target

The only cut used required a non-zero beam current. The basic asymmetry assuming an ABAB sequence for all is 5×10^{-6} . To get a better handle on the systematic error a random number generator was used to randomly determine either an ABBA or BAAB pattern for each run. The 14 sequences were randomly determined 1000 times giving a root mean square of 5×10^{-5} as shown in Fig. 19. The HAPPEX data has a very large data rate so all errors should be systematic. This test has shown that the Lumis should be able to monitor the luminosity differences between target spin up and target spin down for the vertically polarized single spin ^3He experiments to the 5×10^{-5} level.

3.9 The polarized ^3He target

The Hall A polarized ^3He target⁴⁴ was successfully used in its standard configuration for the experiments E94-010⁴⁵ and E95-001⁴⁶ in 1998-1999, E99-117⁴⁷, E97-103⁴⁸ in 2001, E01-012⁴⁹ and E97-110⁵⁰ in 2003.

The standard polarized ^3He target used optically pumped Rubidium vapor to polarize ^3He nuclei via spin-exchange. Two sets of Helmholtz coils provided a 25 Gauss holding field for any direction in the scattering (horizontal) plane. Target cells were up to 40 cm long with density of about 10 amg (10 atm at 0°). Beam currents on target ranged from 10 to 15 μA to keep the beam depolarization effect small and the cell survival time reasonably long (> 3 weeks). The luminosity was about 10^{36} nuclei/s/cm². The in-beam average target polarization achieved was typically over 40%. Two kinds of polarimetry, NMR and EPR (Electron-Paramagnetic-Resonance), were used to measure the polarization of the target. The uncertainty achieved for each method was less than 4% relative and the methods agreed well within errors.

Recent development effort for the approved polarized ^3He experiments, (E02-013, G_E^n ⁴⁰ and E03-004 transversity) has achieved a number of improvements. Most

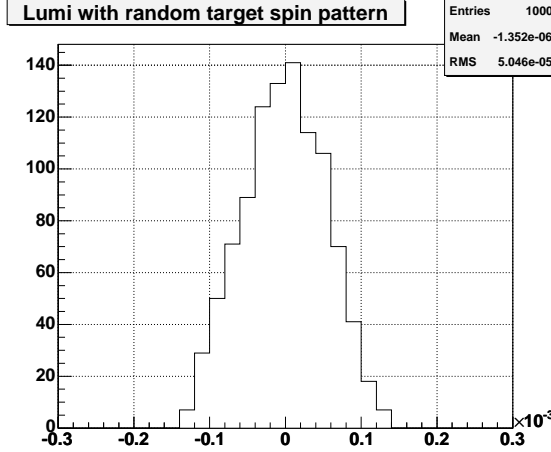


Figure 19: The Asymmetries of the Hall A Lumi sum divided by the BCM with 14 minute time windows for HAPPEX slug 30, using 1000 different random combinations of ABBA or BAAB. The very high rate of HAPPEX experiments means that the RMS is related only to the Lumi systematic error for 14 minute time windows.

significant is the success of the K-Rb hybrid spin-exchange technique⁵¹. Due to the much higher K-³He spin exchange efficiency, the new hybrid cells have significantly shorter spin-up times and improved performance. There are about 10 usable hybrid cells manufactured by the UVa (Gordon Cate's) group and the William and Mary (Todd Averett's) group. Most of the cells have spin-up times of 6-8 hours (to be compared with 20 hours for a typical Rb cell) and polarizations without beam of 45 – 50% (to be compared with 40 – 45% for a typical Rb cell). Also due to the improved spin exchange efficiency, the recent testing results indicate that only about 2/3 of the laser power is needed to achieve the maximum polarization. The success rate of cell manufacturing is also greatly improved since with the much short spin-up time, the requirements on the cell life-time become significantly relaxed.

A new laser building next to the counting house was constructed earlier this year to replace the laser hut in the hall. A new target lab with its infrastructure and safety interlock system has been setup in the new laser building. A new target system (for the G_E^n experiment) has been setup and is being tested in the new target lab. With the laser building moved outside the hall, an optical fiber system is needed to transport the laser light into the hall. Eight 75m-long optical fibers and two 5-to-1 combiners were acquired and tested. The typical light intensity drop through the optical fiber system is about 15%. Air cooling and a temperature interlock system are used to protect the fibers from over-heating. Eight Coherent 30 watts diode laser FAP-system were used for previous experiments (three for longitudinal polarization, three for transverse polarization and two spares). Four of the used Coherent lasers have recently replaced the diodes. Two additional Coherent 60 watts diode laser DUO-FAP were purchased recently. There should be enough lasers and optical components for the next a few planned polarized ³He experiments. including this

proposed measurement.

This experiment requires frequent polarization direction reversal to minimize target-spin-correlated systematic uncertainties. Studies have been performed on this issue. The target spin will be flipped using RF AFP technique and the laser polarization flip will be accomplished with rotating quarter-wave plates. Using AFP RF spin-flip technique, polarization direction reversal was achieved in a time scale of a few seconds. A rotation stage was acquired and was tested to be able to rotate the quarter-wave plate also in a time scale of a few seconds. Due to AFP polarization loss, the maximum polarization will be reduced for frequent spin-flip. The equilibrium polarization P_{eq} is related to the maximum polarization P_{max}

$$P_{eq} = \frac{T_{flip}}{T_{flip} + \delta T_{spin-up}} P_{max}, \quad (19)$$

where T_{flip} and $T_{spin-up}$ are the spin-flip time and the spin-up time correspondingly. δ is the AFP polarization loss for each spin-flip. The frequency of the polarization reversal will be kept to be around 10-20 minutes. It is optimized to keep the maximum polarization while still have target-spin-correlated systematic uncertainties under control. With a spin-flip frequency of 10-20 minutes, a spin-up time of 6 hours, and an AFP loss of 0.3%, the maximum equilibrium polarization will be reduced by 5 – 10% relative (i.e. instead of 45 – 50%, it will be 40 – 45% for 10 minutes flip or 43 – 48% for 20 minutes flip).

For this measurement, a third set of Helmholtz coils is needed to provide a holding and polarization field in the vertical direction. It will be added without taking apart the existing sets of coils. Fig. 20 shows the conceptual design.

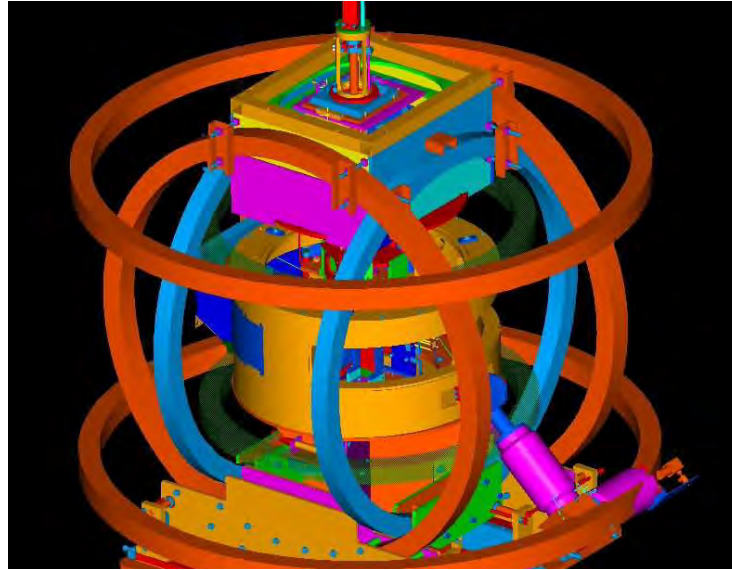


Figure 20: The design of the vertical coils for the polarized ^3He target.

To accommodate optical pumping in the vertical direction, the oven will be tilted to be offset from the center so that the laser light will not overlap with the vertical motion and support mechanism. A mirror will be mounted on top of the pumping chamber to allow the laser light to be reflected into the pumping chamber from the top, as shown in Fig. 21.

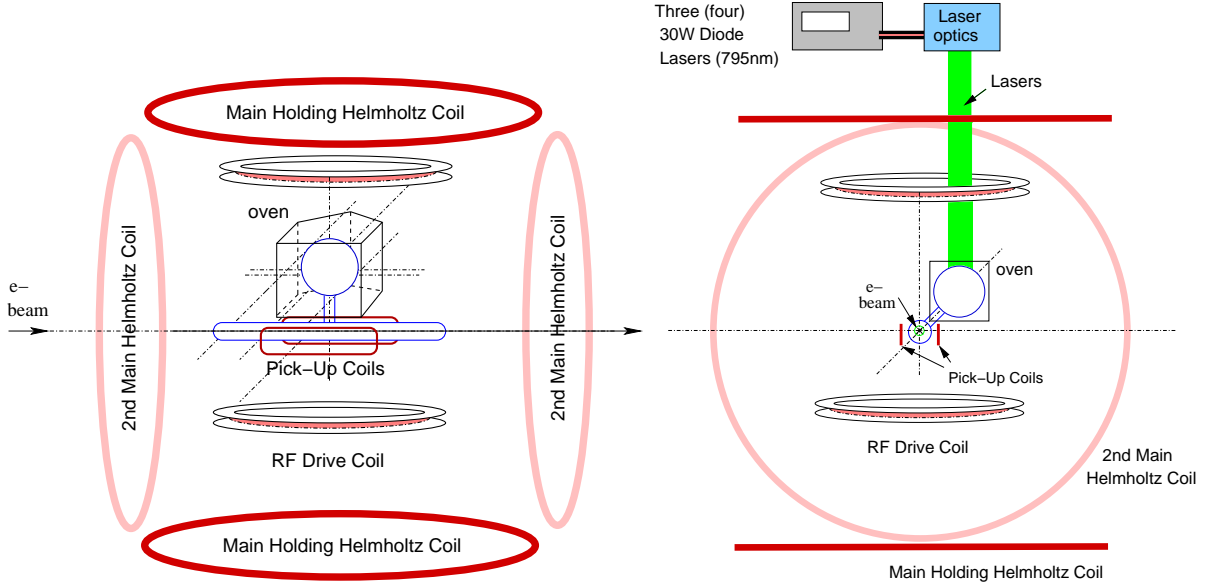


Figure 21: The schematic of the polarized ^3He target, side view (left) and beam view (right).

Effects of BigBite magnetic field

The BigBite magnet will be 1.5 meters away from the target center. Its fringe field can cause a field gradient in the target region. A field clamp will be used to reduce the field gradient. A set of correction coils will be used to further minimize the field gradient. From the experience of running an earlier polarized ^3He experiment E97-110 (Small Angle GDH), which had a significant fringe field from a Septum magnet, using of a field clamp and correction coils reduced the field gradient by an order of magnitude to eliminate possible complications. The BigBite fringe field at the target region is significantly less than that of the Septum in the first run-period of E97-110. The field gradient after the correction is expected to be less than 10 mG/cm, which has a negligible effect on the polarization and a reasonably small effect on the AFP loss.

4 Event Rate Estimate and Statistical Uncertainties

4.1 Cross section and rate estimate

The estimation of the coincidence cross sections has the following inputs:

- The inclusive $p(e, e')$ and $n(e, e')$ cross sections. Deep-inelastic cross sections for ^3He are assumed to be the sum of the two-protons plus one neutron, neglecting the nuclear effects in the intermediate x -region.
- A parameterization of $R = \sigma_L/\sigma_T$, to account for the longitudinal photon polarization.
- Parameterizations of the fragmentation functions D_π^+ and D_π^- for quark to pion fragmentation, D_K^+ , D_K^- and D_d^K for quark to kaon fragmentation.
- A model of the transverse momentum distributions of pion and kaon as fragmentation products.

The inclusive deep inelastic (e, e') cross section can be expressed in the quark parton model as:

$$\frac{d^2\sigma}{d\Omega dE'} = \frac{\alpha^2(1 + (1 - y)^2)}{sxy^2} \frac{E'}{M_N \nu} \sum_{q, \bar{q}} e_q^2 f_1^q(x), \quad (20)$$

where $s = 2E M_N + M_N^2$. The unpolarized quark distribution functions $f_1^q(x)$ and $f_1^{\bar{q}}(x)$ are taken from the CTEQ5M global fits⁵². The semi-inclusive $(e, e'h)$ cross section relates to

the quark fragmentation function $D_q^h(z)$ and the total inclusive cross section σ_{tot} through:

$$\frac{1}{\sigma_{tot}} \frac{d\sigma(e, e'h)}{dz} = \frac{\sum_{q, \bar{q}} e_q^2 f_1^q(x) D_q^h(z)}{\sum_{q, \bar{q}} e_q^2 f_1^q(x)}. \quad (21)$$

For the quark to pion fragmentation functions $D_\pi^+(z)$ and $D_\pi^-(z)$, we follow the parameterization⁵³ of KKP to obtain the sum of $D_\pi^+(z) + D_\pi^-(z)$. For the ratio $D_\pi^-(z)/D_\pi^+(z)$, we use a fit to the HERMES data⁵⁴: $D_\pi^-/D_\pi^+ = (1 - z)^{0.084}/(1 + z)^{1.984}$. Fragmentation functions D_K^+ , D_K^- and D_d^K in the KKP parameterization are used.

Existing data indicate that the fragmented products follow a Gaussian-like distribution in transverse momentum. For the $N(e, e'\pi)X$ reaction, recent HERMES preliminary data showed that the transverse momentum (P_\perp) distribution for both π^+ and π^- follow the form of $e^{(-aP_\perp^2)}$ with $a = 3.76 \text{ (GeV/c)}^{-2}$, corresponding to an average quark transverse momentum of $\langle P_\perp^2 \rangle = 0.26 \text{ (GeV/c)}^2$. Charged kaon transverse momentum distributions are also found to be similar. We used this distribution and realistic spectrometer acceptances in a Monte Carlo simulation to estimate the count rates. The issue of hadron decay is also considered in the rate estimation. The typical survival factors for π^\pm and K^\pm of 2.40 GeV/c momentum are 0.83 and 0.25 correspondingly, after a flight-path of 25.0 m through HRS.

4.2 Cross sections, rates and total number of $(e, e'\pi^-)$ events

The cross sections, event rates and total number of events for each bin are listed in Table-6 for the $(e, e'\pi^-)$ reaction. We have assumed a beam current of 15 μA a target length of 40 cm with a ^3He gas pressure of 10 atm and a target polarization of 42%.

E' GeV	$\Delta E'$ GeV	θ_e deg.	$\langle x \rangle$	$d\sigma_{(e,e')}$ nb/GeV/sr	$d\sigma_{(e,e'\pi^-)}$ nb/GeV ² /sr ²	Rate $_{\pi^-}$ Hz	N_{π^-} k
0.815	0.431	30.0	0.135	29.64	$\theta_\pi = 16.0^\circ, p_\pi = 2.4 \text{ GeV}/c$		
1.246	0.398	30.0	0.225	19.37	7.99	0.17	317.5
1.612	0.340	30.0	0.315	12.95	6.30	0.12	231.1
1.925	0.381	30.0	0.405	8.37	4.46	0.07	139.7
					2.73	0.05	95.8

Table 6: Cross sections, event rates and the total number of events (N_{π^-} in thousands). Data of all x -bins will be collected simultaneously.

Physics asymmetries on ^3He are translated into neutron asymmetries $A_{UT}^{\pi^-}(n)$ and listed in Table 7 together with the corresponding dilution factors. The dilution factor f_{π^-} will be measured by comparing yields from polarized target runs with that of hydrogen reference cell runs. The dilution factors are expected to be measured to $\delta f/f \leq 2\%$ within a relatively short time. An effective neutron polarization of 86.5% in ^3He ground state has been taken into account.

E' GeV	$\langle x \rangle$	R	$B(x)/A(x, y)$	D_{nn}	z_π	f_{π^-}	$1/f_{\pi^-} P_T P_n \sqrt{N_{\pi^-}}$ %
0.815	0.135	0.32	0.249	0.267	0.46	0.33	1.47
1.246	0.225	0.26	0.375	0.398	0.51	0.31	1.82
1.612	0.315	0.21	0.485	0.501	0.55	0.30	2.46
1.925	0.405	0.18	0.584	0.582	0.59	0.29	3.03

Table 7: The expected statistical uncertainties of the single spin asymmetry $A_{UT}^{\pi^-}(n)$ are listed with the corresponding dilution factors f_{π^-} , $R = \sigma_L/\sigma_T$, and the Collins kinematic factor $B(x)/A(x, y)$. The ideal Collins kinematic factor D_{nn} are also listed as a comparison.

4.3 Statistical uncertainties of Collins and Sivers moments for π^- and K^- production

With a full 2π coverage of the Collins angles and almost 2π coverage of Sivers angle, this experiment can make clear separation of Collins asymmetries from Sivers asymmetries. For each kinematic bin, we need to find the best fit of parameters a

and b for an event-probability distribution:

$$y_i(\phi_h^i, \phi_S^i) = \frac{1}{NV(\phi_h^i, \phi_S^i)} \left[1 + a \sin(\phi_h^i + \phi_S^i) + b \cdot \sin(\phi_h^i - \phi_S^i) \right] \quad (22)$$

in which N is the number of event. The relative phase space volume $V(\phi_h^i, \phi_S^i)$ can be obtained from target-spin-averaged counts. The details of asymmetry separations and statistical uncertainties are provided in Appendix-III. The expected statistical uncertainties on the overall target SSA $A_{UT}^{n\pi^-}$, and separated into the Collins asymmetry $A_{UT}^{n\pi^- Collins}$ and the Sivers asymmetry $A_{UT}^{n\pi^- Sivers}$ are listed in Table 4.3 for the $n^\uparrow(e, e'\pi^-)$ measurements.

$\langle x \rangle$	$\delta A_{UT}^{n\pi^-}$ %	$\delta A_{UT}^{n\pi^- Collins}$ %	$\delta A_{UT}^{n\pi^- Sivers}$ %
0.135	1.47	2.56	2.56
0.225	1.82	2.78	2.78
0.315	2.46	3.52	3.52
0.405	3.03	4.27	4.27

As by-products, target SSA in $n^\uparrow(e, e'K^-)$ reaction will also be measured. The corresponding total number of events, dilution factors and statistical uncertainties on $A_{UT}^{nK^-}$, and uncertainties of its Collins and Sivers moments are listed in Table. 8.

$\langle x \rangle$	f_{K^-}	N_{K^-} k	$\delta A_{UT}^{nK^-}$ %	$\delta A_{UT}^{nK^- Collins}$ %	$\delta A_{UT}^{nK^- Sivers}$ %
0.135	0.33	39.1	4.16	7.24	7.24
0.225	0.31	25.2	5.54	8.48	8.48
0.315	0.29	14.1	8.12	11.61	11.61
0.405	0.26	9.1	10.95	15.44	15.44

Table 8: The expected number of events (N_{K^-}) in $(e, e'K^-)$ channel, the corresponding dilution factor f_{K^-} , statistical uncertainties of $A_{UT}^{nK^-}$, and statistical uncertainties of Collins and Sivers moments of K^- production on a neutron.

4.4 Systematic uncertainties

The experimental uncertainties on SSA will be dominated by statistical uncertainties. We discuss several possible sources of systematic uncertainties in this section.

Effective nucleon polarization in ^3He

Effective nucleon polarization in ^3He for deep-inelastic scattering gives:

$$g_1^{3He} = P_n g_1^n + 2P_p g_1^p \quad (23)$$

where $P_n(P_p)$ is the effective polarization of the neutron (proton) inside ^3He ⁵⁵. These effective nucleon polarizations $P_{n,p}$ can be calculated using ^3He wave functions constructed from N-N interactions, and their uncertainties were estimated using various nuclear models ^{56,55,57,58}, giving

$$P_n = 0.86^{+0.036}_{-0.02} \text{ and } P_p = -0.028^{+0.009}_{-0.004}. \quad (24)$$

The small proton effective polarization (2.8%) causes small offsets in the ^3He asymmetries, compared to that from a free neutron. The uncertainties associated with this small offset are even smaller when considering that the corresponding proton asymmetries are better known with the HERMES data.

Corrections to A_{UT} due to target polarization drifts

The systematic uncertainties due to the target polarization measurements contribute to $\pm 4\%$ relative uncertainties to the systematics of A_{UT} .

The target polarization between spin up and spin down runs may not be exactly the same. A drift in the target polarization does not cause any single-spin asymmetry itself, but results in a small change which is easy to correct. Assuming the yield is: $\sigma = \sigma_0 + P_T \sigma_1$ for target spin up and spin down, we have: $\sigma_+ = \sigma_0 + P_T \sigma_1$ and $\sigma_- = \sigma_0 - P_T \sigma_1$. The measured asymmetry is:

$$A_0 = \frac{\sigma_+ - \sigma_-}{\sigma_+ + \sigma_-} = P_T \frac{\sigma_1}{\sigma_0}. \quad (25)$$

If during spin down runs the average target polarization changes to $P_T + \delta P_T$, such that $\sigma'_+ = \sigma_0 + P_T \sigma_1$ and $\sigma'_- = \sigma_0 - (P_T + \delta P_T) \sigma_1$, the measured asymmetry changes to:

$$A' = \frac{\sigma'_+ - \sigma'_-}{\sigma'_+ + \sigma'_-} = A_0 \frac{1 + \frac{\delta P_T}{2P_T}}{1 - \frac{\delta P_T}{2P_T} \cdot A_0}. \quad (26)$$

Since $A_0 \delta P_T / 2P_T \ll 1$, we have:

$$A' \approx A_0 \left(1 + \frac{\delta P_T}{2P_T}\right) \left(1 + \frac{\delta P_T}{2P_T} \cdot A_0\right) \approx A_0 \left(1 + \frac{\delta P_T}{2P_T}\right). \quad (27)$$

As long as the target polarization is measured, the drifts in average polarization between spin up and spin down runs will not cause any significant uncertainty in A_{UT} .

Pions from exclusive ρ production

Pions from exclusive ρ production can be a possible source of contamination. However, at the kinematics of this experiment such contaminations are negligible. Recent Hall C E00-108 experiment ³⁶, which run at a similar kinematics as this experiment,

has estimated the exclusive ρ contributions to the SIDIS cross section, the results are shown in Fig. 22, the difference between open symbols and filled symbols (ρ contribution subtracted) are very small at $z \approx 0.5$.

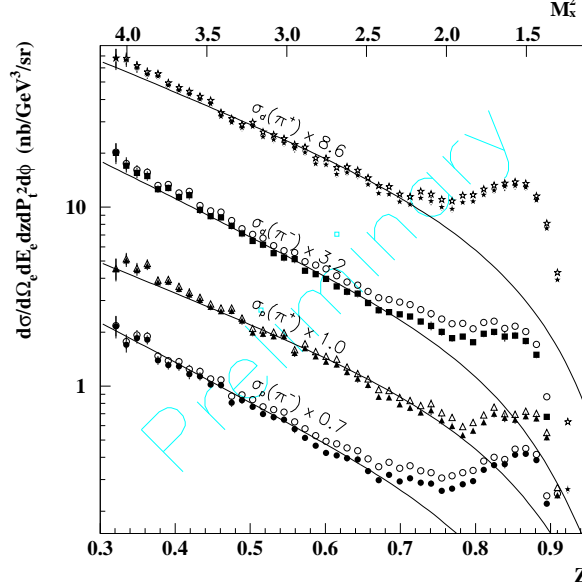


Figure 22: Hall C E00-108 experiment ³⁶, the difference between open symbols and filled symbols corresponds to exclusive ρ contribution.

Other terms in SSA and cross sections

The $\sin(3\phi_h - \phi_S)$ term in Eq. 7 is expected to be rather small since it involves not only transverse-momentum-dependent distribution functions ($h_{1T}^{\perp q}$) but also the Collins fragmentation functions (H_1^\perp). The coverage of ϕ_h in this experiment is close to 180° for most x -bins, therefore, we expect all $2\phi_h$ and $3\phi_h$ terms to be averaged out nicely. Any significant angular dependence (such as $\cos(2\phi)$ terms) of spin independent cross sections can be easily identified and corrected for within the experimental acceptance. The experimental phase space in ϕ_h can be determined from a Monte Carlo simulation cross checked with uncorrelated single-arm events.

5 Beam time request, hardware costs and installation time needed

5.1 Beam time request

The beam time request are listed in Table 9. We request 576 hours (24 days) of total beam time, of which 528 hours is for beam on the polarized ^3He target. Overhead time of 48 hours total is requested. This overhead time can be shared between activities such as unpolarized target runs, target spin flip and target polarization measurements, as has been done in the past during other Hall A polarized ^3He target

experiments. Major target related down times can also be arranged to coincide with the scheduled accelerator maintenance activities in order to save overhead time.

Table 9: Beam time request.

	Time (Hour)
Production on Pol. ^3He	528
Reference cell runs, optics and detector check	16
Target Overhead: spin rotation, polarization measurement	32
Total Time Request	576 (24 days)

Table 10: Details of the beam time request.

5.2 Hardware costs and installation time needed

All major hardware components required in this experiment, including the target, spectrometers and detectors are either already standard Hall A equipments or about to become the standard Hall A equipments. The BigBite spectrometer together with its electron detection package is scheduled to be commissioned in February 2006 for the G_{En} experiment. This proposal has no additional requirement on the BigBite detectors beyond its expectation for the G_{En} experiment.

We will be using the standard hall A polarized ^3He target with upgrade to have vertical polarization capabilities. The vertical target magnet coils, together with a new oven for pumping cell, mechanical support, laser optics and new target cells add up the cost to be about \$100 k.

The overall installation time needed for this experiment is estimated to be between four to six weeks. Installation of the Hall A polarized ^3He target can be accomplished within two to three weeks. The installation time needed for the BigBite spectrometer, depends on the sequence of experiments, can be two to three weeks.

6 Expected Results and Impacts

The expected statistical accuracies Collins and Sivers moments (as defined in Eq. 11-12) of neutron are plotted in Fig. 23. HERMES (published²¹ and 2005-preliminary²²) and COMPASS²⁴ A_{UT} data are also shown as a comparison. The accuracy on neutron A_{UT} data from this experiment will be comparable to that of the published HERMES proton data, and much improved over the COMPASS deuteron data which currently holding all our knowledge of neutron SSA. This experiment will extend the neutron SSA measurement to the valence quark region where effects of

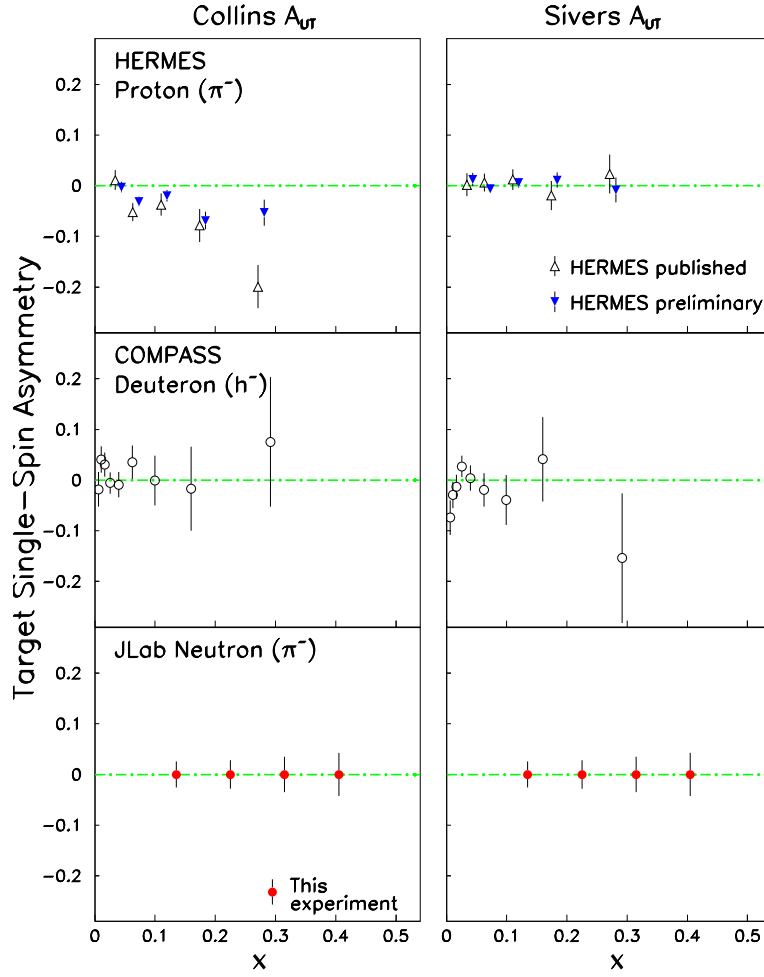


Figure 23: The projected JLab data of target single spin asymmetry A_{UT} for both Collins and Sivers moments in $n^\uparrow(e, e' \pi^-)$ reaction are compared with HERMES^{21,22} and COMPASS²⁴ A_{UT} data.

quark transversity are expected to become important and is beyond the kinematics reach of the COMPASS experiment.

Determining the sign of the neutron Collins moments in $n^\uparrow(e, e'\pi^-)$ reaction is a crucial step toward resolving the much puzzled relationship between the favored ($H_1^{\perp fav}$) and the unfavored ($H_1^{\perp unfav}$) Collins fragmentation functions. In a simplified manner, we have Collins $A_{UT}^{n\pi^-} \propto 4\delta d \cdot H_1^{\perp unfav} + \delta u \cdot H_1^{\perp fav}$. Since one expects δd is small and negative compared to δu , much like Δd to Δu , a positive Collins moment $A_{UT}^{n\pi^-}$ will clearly indicate the domination of the favored Collins function. If on the other hand the Collins $A_{UT}^{n\pi^-}$ turns out to be negative, a large unfavored Collins function with the opposite sign could be the only explanation. With this experiment providing the first direct neutron data, a combined analysis with the HERMES proton data will be able to constrain four pieces of unknowns in the Collins asymmetries: quark transversity δu and δd and Collins fragmentation functions $H_1^{\perp fav}$ and $H_1^{\perp unfav}$.

Collins moments of neutron in $n^\uparrow(e, e'\pi^-)$ reaction are compared with the parameterization of Vogelsang and Yuan²⁵ in Fig. 24. Since Vogelsang and Yuan²⁵ concluded that $H_1^{\perp fav} \approx -H_1^{\perp unfav}$, their parameterization predicts small values for the neutron Collins moments due to the cancellations between u and d -quarks. On the other hand, if one assumes unfavored and favored Collins functions follow approximately $H_1^{\perp unfav}/H_1^{\perp fav} \approx D_1^{unfav}/D_1^{fav}$, a sizable Collins asymmetry is expected as shown in Fig. 24 from a PQCD model calculation⁴ of Ma, Schmidt and Yang at the kinematics of this experiment. Recent Belle results indicated that $H_1^{\perp unfav}$ is opposite in sign to $H_1^{\perp fav}$, but much smaller, more in line with the earlier model's assumption.

Sivers moments of neutron in $n^\uparrow(e, e'\pi^-)$ reaction are compared with the parameterization of Anselmino *et al.*²⁶ and Vogelsang and Yuan²⁵ in Fig. 25. In a simplified manner, we have the Sivers $A_{UT}^{n\pi^-} \propto 4f_{1T}^{\perp(1)d} \cdot D_1^{unfav} + f_{1T}^{\perp(1)u} \cdot D_1^{fav}$. At the kinematics of this experiment, the regular fragmentation functions are well-known and the ratio is $D_1^{unfav}/D_1^{fav} \approx 1/3$. Therefore, for this experiment we have Sivers $A_{UT}^{n\pi^-} \propto \frac{4}{3}f_{1T}^{\perp(1)d} + f_{1T}^{\perp(1)u}$. The sign and magnitude of the neutron Sivers moment $A_{UT}^{n\pi^-}$ will be crucial inputs to obtain information on quark angular momentum. If Sivers $A_{UT}^{n\pi^-}$ turns out to be positive, the same sign as in the proton Sivers $A_{UT}^{p\pi^+}$, then the u -quark Sivers function should be much larger than the d -quark Sivers, indicating a large positive angular momentum carried by the u -quark. If on the other hand the Sivers $A_{UT}^{n\pi^-}$ turn out to be negative, as predicted by Anselmino *et al.* and Vogelsang and Yuan, a large d -quark Sivers function with opposite sign to u -quark is needed, indicating that d -quark carries a rather large angular momentum opposite to the nucleon spin.

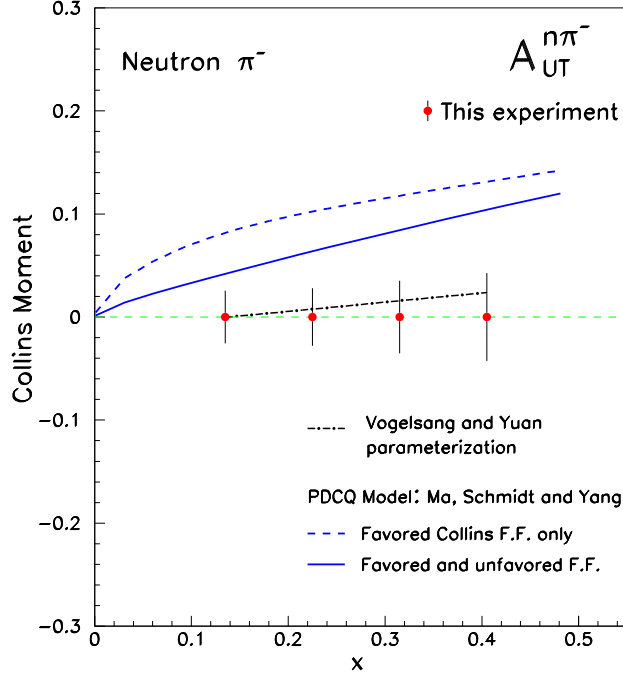


Figure 24: The projected JLab data of neutron Collins moments are compared with the parameterization of Vogelsang and Yuan²⁵ and model predictions of Ma, Schmidt and Yang⁴.

7 Relation with other experiments

This neutron SIDIS SSA measurement is complementary to the HERMES proton and the COMPASS deuteron measurements. COMPASS experiment is at low x region than this measurement. HERMES is at similar x region. The combined neutron and proton measurements will allow a detailed study of the flavor structure of the Collins and Sivers moments. Bella $e^+e^- \leftarrow \pi\pi$ measurements will help to extract the Collins fragmentation functions, which will be crucial for extracting the transversity distributions from the Collins moments. This study of the transverse SSA in SIDIS is closely related to the transverse SSA study at RHIC with $p-p$ colliding and in the future at PAX with $p-\bar{p}$ colliding⁵⁹. The RHIC-spin will probe low x region at high energies. PAX at GSI can provide a clean method to measure transversity with Drell-Yan process. It is expected to start data taking in 2014 for phase I and later for phase II when the transversity program is planned. Both RHIC-spin and PAX are complementary to the SIDIS program. This measurement should open up a window for SSA in SIDIS at JLab, and is particularly important for future SIDIS program with the 12 GeV upgrade and with the future EIC facility.

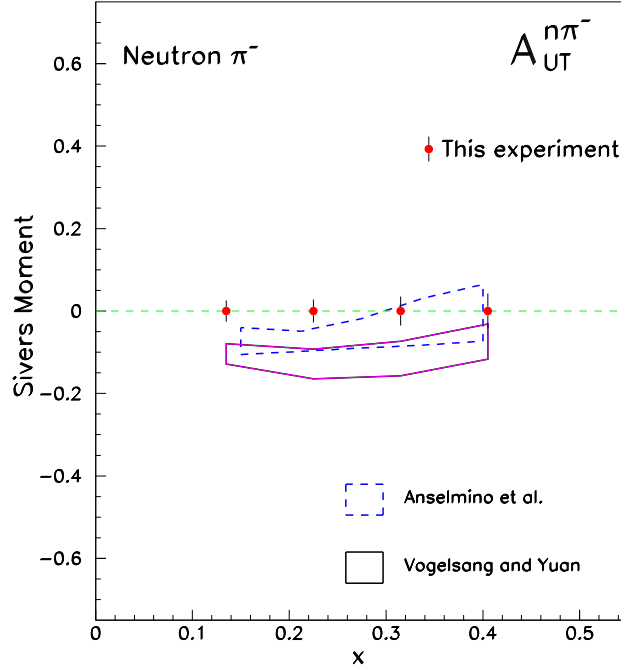


Figure 25: The projected JLab data of neutron Sivers moments are compared with the parameterization of Anselmino *et al.*²⁶ and Vogelsang and Yuan²⁵.

8 Manpower and collaboration

The core group of the collaboration has grown significantly. Four students have been identified as PhD candidates for this transversity experiment. Two have been stationed at JLab for a year: Huan Yao (from Temple University) has been working on the testing and upgrading of the polarized ^3He target and Xin Qian (from Duke University) has been focused on GEANT simulation of the BigBite background. Two other students have been at JLab for several months and will be stationed at JLab starting in March of 2006: Chiranjib Dutta and Allada Kalyan from University of Kentucky have helped working on the polarized ^3He target and the BigBite detector system. A post-doc, Dr. Lingyan Zhu from UIUC, has been nearly full time working on the preparation of the experiment for more than a year. Another post-doc, Dr. Tim Holmstrom from William and Mary has been working on the polarized ^3He target and also analyzed the lumi data. New groups, which have experience analyzing HERMES data, joined the experiment. The theoretical support is significantly enhanced with the addition of two theory groups who are active in this topic.” Two other polarized ^3He experiments, (e,e’d) experiment and A_y , will fit nicely together with this experiment as a group to run as was in the very preliminary (informal) planning of Hall A running schedule. The combined manpower contains a lot of experience on the polarized ^3He , the BigBite and HRS system.

9 Summary

On the frontier of recent research activities to understand the nucleon structure and QCD is the study of the transverse spin distributions and transverse spin phenomena. Although still in its infancy, the experimental study of transverse spin physics has generated great theoretical excitement. Recent theoretical activities have gone beyond just the transversity distributions. The other transverse spin phenomena, such as the Sivers functions, have shed light on some difficult aspects of the nucleon structure and QCD. The Sivers mechanism helps to understand quark orbital angular momentum and also links many different hadronic physics reactions together.

New results from HERMES for the proton and COMPASS for the deuteron show a strong and unexpected flavor dependence of the transverse spin asymmetries. With high luminosity 6 GeV beam and a polarized ^3He target with flexible polarization directions, JLab is in an ideal position to make an important contribution in this endeavor. The recent SIDIS data show that the factorization works reasonably at the optimized JLab kinematics. We propose a first measurement of SIDIS π^- production on the neutron with a transversely polarized ^3He target. It will provide first set of cleanly separated Collins and Sivers asymmetries on the neutron in the x range of 0.13 to 0.41, which will provide powerful constraints on the transversity distributions and Sivers functions for both u and d -quarks in the valence region. This experiment will be the first transverse target SIDIS experiment at Jefferson Lab, and will begin a new era of spin physics at JLab. The program of transverse spin and transversity physics will flourish with the 12 GeV upgrade and the future EIC program.

Great progress has been made since the approval of the initial E03-004 proposal. Experimental equipment (BigBite, Polarized ^3He , HRS detectors, Lumi detectors) has significantly progressed; it is very well established that this experiment can be accomplished as proposed. Experimental conditions are optimized. The core collaboration, especially the PhD students and post-docs, has been working earnestly on preparations for the experiment, and is eagerly waiting for the experiment to be scheduled. We request the PAC to re-approve the experiment for 24 days of beam time with a high scientific rating.

10 Acknowledgment

We thank W. Vogelsang and F. Yuan, M. Anselmino and A. Prokudin for providing calculations of their parameterizations for the kinematics of the proposed measurements.

A Appendix-I. PAC23 report on E03-004

Individual Proposal Report

Proposal: PR-03-004

Scientific Rating: B+

Title: Measurement of Single Target-Spin Asymmetry in Semi-Inclusive Pion Electroproduction on a Transversely Polarized ^3He Target

Spokespersons: X. Jiang, J. P. Chen, and J-C. Peng

Motivation: Measurements of Single Spin Asymmetries (SSA) have been shown to be a powerful tool, with the potential to access new and unmeasured partonic distribution functions, including transversity. The first promising results are becoming available. A worldwide program is currently running or planned, using proton and deuteron targets, several probes, and various choices of kinematics. This proposal aims to perform the first measurement of SSA using electrons on a neutron target, the latter provided by polarized ^3He .

Measurement and Feasibility: It is proposed to measure the azimuthal distribution of π^- in the reaction $^3\text{He}(e, e'\pi^-)X$ with a polarized helium target in Hall A. A 6 GeV beam will be used together with the BigBite spectrometer to detect electrons and an HRS spectrometer to detect the pions close to the virtual photon direction. The Hall A polarized helium target, which has already been successfully used in other experiments, will be modified to allow complete freedom in choosing the polarization direction and to permit frequent flipping of the spin. The measurement appears to be feasible, if the effects that acceptance cuts have on the extracted pion distributions are kept under control. The overall systematic uncertainty of the planned measurement may be larger than projected, but still would be less than the statistical uncertainties and therefore would be acceptable for a first measurement.

Issues: Since factorization may be questionable at 6 GeV, the interpretation of the measured asymmetry in terms of the convolution of distribution and fragmentation functions may be problematical. To improve the likelihood of a successful simplified analysis, the PAC recommends that the measurement be undertaken at larger values of z , namely $z \cong 0.5$ and 0.6 , instead of the proposed values of $z \cong 0.4$ and 0.5 . It is also noted that additional contributions can enter into the asymmetry. They may come from interferences between transverse and longitudinal projection of the current matrix elements in the reaction. While these are usually assumed to be negligible when compared with the purely transverse response, at the lowest values of Q^2 proposed, they may play some role. The analysis should be done in a way that allows for the different azimuthal angle dependences these contributions imply.

Recommendation: Approve for 24 days in Hall A

B Appendix-II. Simulation of BigBite background rates and comparisons with test runs

We used a GEANT3 based simulation code ⁴¹ to study the background rates on BigBite detectors. The event generator uses photon-nuclear fragmentation package DINREG to substitute the original code PFIS. The electron-nuclear interactions are modeled using equivalent photon representation of an electron ⁴¹. The same simulation code was used earlier for many JLab experiments to address issues related to background rates. The simulation code usually tends to over-estimate background rates by a factor of 2-3.

We compared background rate data in three experimental situations with the simulation. After confirming the reliability of the simulation, we extended our background simulation to the situation of BigBite detectors in the G_E^n experiment and in the “neutron transversity” experiment.

The first comparison with data is for a BigBite test run taken in April, 2005, during the Short Range Correlation (SRC) experiment. The beam was 4.63 GeV at a current of 2 μ A. The target was a 4 cm LD₂ cell. The BigBite is located at 99°, 1.0 meter away from the target. The BigBite magnetic field was 0.986 T in negative mode. The simulation reproduce rates on three different scintillator planes to within 50%, for both cases of magnet on (Fig. 26) and magnet off (Fig. 27).

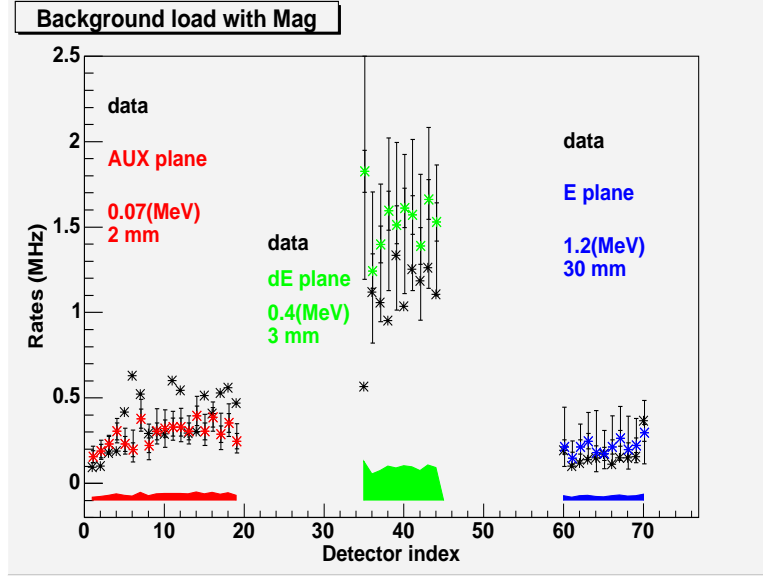


Figure 26: Rates comparison between test data and simulation with BigBite magnet turned on during the SRC experiment. Scintillator thickness and cut offs in simulated energy deposit are indicated for each plane. The points with error bars are from the simulator. The inner error bars show the statistical uncertainty of the simulation. The outer error bars correspond to the systematics uncertainty due to the threshold cuts in the test data analysis. The color bands show the systematics due to the uncertainties of the geometry.

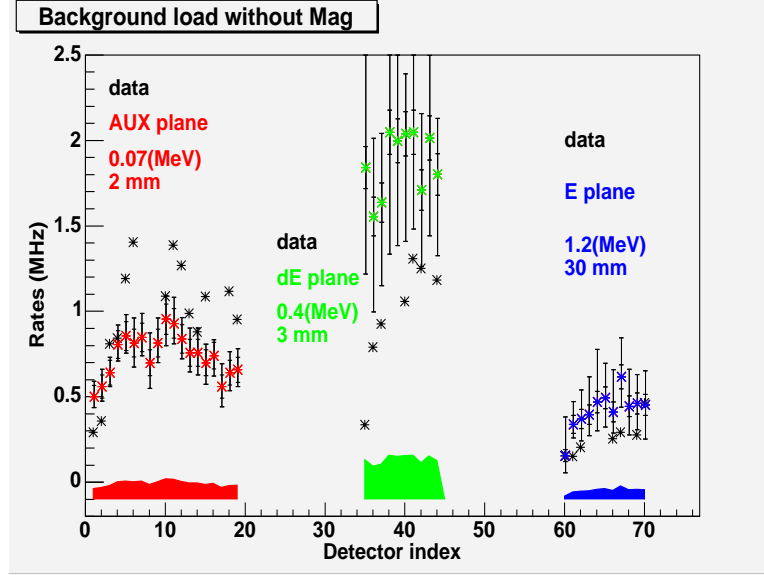


Figure 27: Simulation compare with test run rates. Same as in Fig. 26, but with the BigBite dipole magnet turned off.

The second comparison is between the SRC production data and the simulation. The beam energy was 4.6 GeV and the current was $8.2 \mu\text{A}$. The target was a tilted Carbon foil with a thickness of 42.3 mg/cm^2 . BigBite is at 99 degrees with 1.0 meter drift distance. The background rates from data is 70 kHz. The simulation result is $181.6 \pm 7.6(\text{stat}) \pm 30.5(\text{sys}) \text{ kHz}$. The systematic error include uncertainties in geometry, threshold cuts, etc. The simulation overestimate the rates by a factor of two.

The third comparison is between a BigBite wire chamber test run and the simulation. The beam energy was 2.75 GeV and the current was $8 \mu\text{A}$. Only the first wire chamber was used in the test run without any magnet. The chamber was located at 70 degree at a distance of 10 meter. The data showed a background rates of 1.8 kHz/wire. At a cut of 1 keV for energy deposit on the wire chamber, the simulation overestimated the data by a factor of 5. At an energy deposit cut of 5 keV, the simulation agreed with the data.

We then extended our simulation to the situation of the G_E^n experiment and the “transversity” experiment. The rates are obtained with shielding protection as illustrated in Fig. 16. In the “transversity” experiment, the beam energy is 6.0 GeV; the beam current is $15 \mu\text{A}$ and the target is a $40 \text{ cm}^3 \text{ He}$ cell; the BigBite is at 30 degrees with 1.5 m drift. In the G_E^n experiment, the beam was 3.2 GeV at a current of $15 \mu\text{A}$ on a ^3He cell; the BigBite is at 54 degrees with 1.1 m drift distance. The rate results are listed in Table 11. The rates for the “transversity” experiment and the G_E^n experiment are similar, with an overall rate no more than 10-20 MHz per chamber.

Experiment	G_E^n Test run	Transversity	GEN
data	1.8 kHz/wire	(per chamber)	(per chamber)
simulation (5 keV cut)	$1.76 \pm 0.12 \pm 0.57$ kHz	7.5 ± 1.7 MHz	6.87 ± 1.62 MHz
simulation (1 keV cut)	$9.88 \pm 0.29 \pm 3.2$ kHz	20.2 ± 2.8 MHz	12.6 ± 2.2 MHz

Table 11: Wire chamber rate estimation for the G_E^n and the “transversity” experiment corresponding to 5 keV and 1 keV energy deposit cut in the simulation.

C Appendix-III. Separation of Collins and Sivers asymmetries

For the events within each kinematic bin, we need to find parameters a and b which maximize the likelihood function:

$$L = \frac{1}{N} \prod_i \frac{1}{V(\phi_h^i, \phi_S^i)} \left[1 + a \sin(\phi_h^i + \phi_S^i) + b \sin(\phi_h^i - \phi_S^i) \right]. \quad (28)$$

in which N is the number of event. The relative phase space volume $V(\phi_h^i, \phi_S^i)$ at bin (ϕ_h, ϕ_S) can be obtained from the target-spin-averaged counts normalized in a way such that $\sum_i 1/V(\phi_h^i, \phi_S^i) = N$. The best fit parameters a and b satisfy two linear equations⁶⁰:

$$\begin{aligned} \frac{a}{N} \sum_i \frac{\sin^2(\phi_h^i + \phi_S^i)}{V(\phi_h^i, \phi_S^i)} + \frac{b}{N} \sum_i \frac{\sin(\phi_h^i + \phi_S^i) \sin(\phi_h^i - \phi_S^i)}{V(\phi_h^i, \phi_S^i)} &= \frac{1}{N} \sum_i \frac{\sin(\phi_h^i + \phi_S^i)}{V(\phi_h^i, \phi_S^i)}, \\ \frac{a}{N} \sum_i \frac{\sin(\phi_h^i + \phi_S^i) \sin(\phi_h^i - \phi_S^i)}{V(\phi_h^i, \phi_S^i)} + \frac{b}{N} \sum_i \frac{\sin^2(\phi_h^i - \phi_S^i)}{V(\phi_h^i, \phi_S^i)} &= \frac{1}{N} \sum_i \frac{\sin(\phi_h^i - \phi_S^i)}{V(\phi_h^i, \phi_S^i)} \end{aligned} \quad (29)$$

The solutions are:

$$a = \frac{1}{\Delta} \left[\beta \cdot \frac{1}{N} \sum_i \frac{\sin(\phi_h^i + \phi_S^i)}{V(\phi_h^i, \phi_S^i)} - \gamma \cdot \frac{1}{N} \sum_i \frac{\sin(\phi_h^i - \phi_S^i)}{V(\phi_h^i, \phi_S^i)} \right], \quad (30)$$

$$b = \frac{1}{\Delta} \left[\alpha \cdot \frac{1}{N} \sum_i \frac{\sin(\phi_h^i - \phi_S^i)}{V(\phi_h^i, \phi_S^i)} - \gamma \cdot \frac{1}{N} \sum_i \frac{\sin(\phi_h^i + \phi_S^i)}{V(\phi_h^i, \phi_S^i)} \right], \quad (31)$$

in which

$$\alpha = \frac{1}{N} \sum_i \frac{\sin^2(\phi_h^i + \phi_S^i)}{V(\phi_h^i, \phi_S^i)}, \quad \beta = \frac{1}{N} \sum_i \frac{\sin^2(\phi_h^i - \phi_S^i)}{V(\phi_h^i, \phi_S^i)}, \quad (32)$$

$$\gamma = \frac{1}{N} \sum_i \frac{\sin(\phi_h^i + \phi_S^i) \sin(\phi_h^i - \phi_S^i)}{V(\phi_h^i, \phi_S^i)}, \quad \Delta = \alpha \cdot \beta - \gamma^2. \quad (33)$$

The one standard deviation⁶⁰ of parameter a and b are given by:

$$\sigma_a = \frac{1}{\sqrt{N}} \cdot \sqrt{\frac{\beta}{\Delta}}, \quad \sigma_b = \frac{1}{\sqrt{N}} \cdot \sqrt{\frac{\alpha}{\Delta}}. \quad (34)$$

An illustration of Collins and Sivers asymmetry separation is shown in Fig. 28. For a Monte Carlo generated event sample with $a = 0.05$ and $b = 0.45$ for neutron, the input values are successfully recovered from the 2D-fit procedure within the statistical uncertainties.

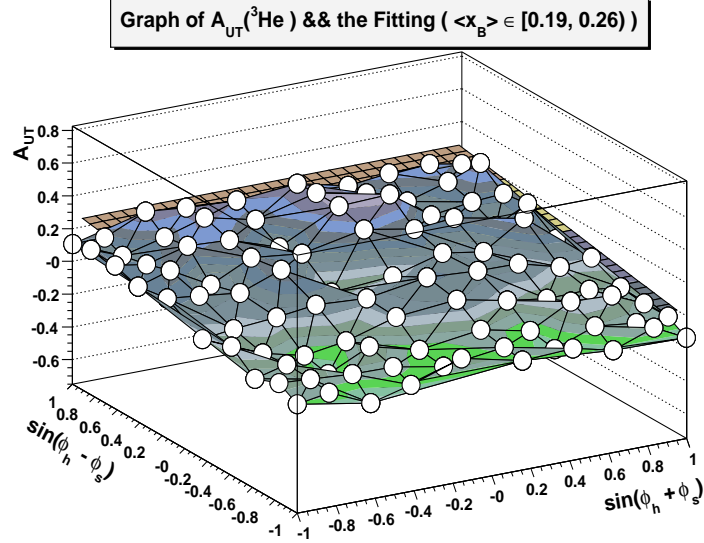


Figure 28: An illustration of 2D-fit on Monte Carlo generated data to separate Collins and Sivers asymmetries.

References

1. J. P. Ralston and D. E. Soper, Nucl. Phys. **B152**, 109 (1979).
2. X. Artru and M. Mekhfi, Z. Phys. **C45**, 669 (1990).
3. P. Schweitzer *et al.*, Phys Rev. **D64**, 034013 (2001).
4. B. Q. Ma, I. Schmidt and J. J. Yang, Phys Rev. **D65**, 034010 (2002), and B. Q. Ma private communications, 2005.
5. J. C. Collins, Nucl. Phys. **B396**, 161 (1993).
6. A. Bacchetta, R. Kundu, A. Metz and P. J. Mulders, Phys. Lett. **B506**, 155 (2001); Phys. Rev. **D65**, 094021 (2002); L. P. Gamberg, G. R. Goldstein and K. A. Oganessyan, Phys. Rev. **D68**, 051501 (2003); A. Bacchetta, A. Metz and J. J. Yang, Phys. Lett. **B574**, 225 (2003); D. Amrath, A. Bacchetta and A. Metz, Phys. Rev. **D71**, 114018 (2005).
7. A. Schaefer and O. V. Teryaev, Phys. Rev. **D61**, 077903 (2000).
8. K. Abe *et al.*, arXiv:hep-ex/0507063.
9. D. Sivers, Phys. Rev. **D43**, 261 (1991).
10. S. J. Brodsky, D. S. Hwang and I. Schmidt, Phys. Lett. **B530**, 99 (2002); Nucl. Phys. **B642**, 344 (2002).
11. J. C. Collins, Phys. Lett. **B536**, 43 (2002).
12. X. Ji and F. Yuan, Phys. Lett. **B543**, 66 (2002); A. V. Belitsky, X. Ji and F. Yuan, Nucl. Phys. **B656**, 165 (2002).
13. D. Boer, S. J. Brodsky and D. S. Hwang, Phys. Rev. **D67**, 054003 (2003).
14. L. P. Gamberg, G. R. Goldstein and K. A. Oganessyan, Phys. Rev. **D67**, 071504 (2003).
15. A. Bacchetta, A. Schaefer and J. J. Yang, Phys. Lett. **B578**, 109 (2004).
16. Z. Lu and B. Q. Ma, Nucl. Phys. **A741**, 200 (2004).
17. F. Yuan, Phys. Lett. **B575**, 45 (2003).
18. P. V. Pobylitsa, hep-ph/0212027
19. A. Airapetian *et al.*, Phys. Rev. Lett. **84**, 4047 (2000); A. Airapetian *et al.*, Phys. Rev. **D64**, 097101 (2001); A. Airapetian *et al.*, Phys. Lett. **B562**, 182 (2002).
20. D. Boer and P. J. Mulders, Phys. Rev. **D57**, 5780 (1998).
21. A. Airapetian *et al.*, Phys. Rev. Lett. **94**, 012002 (2005).
22. M. Dieffenthaler, arXiv:hep-ex/0507013.
23. Alessandro Bacchetta, Umberto D'Alesio, Markus Diehl, C. Andy Miller, *Phys. Rev. D* **70**, 117504 (2004).
24. V. Y. Alexakhin *et al.*, Phys. Rev. Lett. **94**, 202002 (2005).
25. W. Vogelsang and F. Yuan, Phys. Rev. **D72**, 054028 (2005).
26. M. Anselmino *et al.*, Phys. Rev. **D72**, 094007 (2005).
27. J. C. Collins *et al.*, arXiv:hep-ph/0509076.
28. O. Martin *et al.*, Phys. Rev. **D57**, 3084 (1998); **D60**, 117502 (1999).
29. J. Soffer, Phys. Rev. Lett. **74**, 1292 (1995).
30. X. Artru, J. Czyzewski and H. Yabuki, Z. Phys. **C73**, 527 (1997).

31. M. Anselmino *et al.*, arXiv:hep-ph/0511017.
32. M. Burkardt, Phys. Rev. **D66**, 114005 (2002); Nucl. Phys. **A735**, 185 (2004).
33. A. Bacchetta, hep-ph/0307282.
34. Xiangdong Ji, Jian-Ping Ma and Feng Yuan, hep-ph/0404183.
35. Xiangdong Ji, Jian-Ping Ma and Feng Yuan, hep-ph/0405085.
36. R. Ent, H. Mkrtchyan and P. Bosted, private communications.
37. C. J. Bebek, *et al.*, Phys. Rev. Lett. **30**, 624 (1973).
38. G. Drews, *et al.*, Phys. Rev. Lett. **41**, 1433 (1978).
39. H. Avakian, for the CLAS Collaboration, the proceeding of the “X-th Workshop on High Energy Spin Physics”, September 16-20, 2003.
40. JLab E02-013, Spokespersons, G. Cates, K. McCormick, B. Reitz and B. Wojtsekhowski.
41. P. V. Degtiarenko, private communications, 2005, and P. V. Degtyarenko, “Applications of the Photonuclear Fragmentation Model to Radiation Protection Problems”. Proceedings of the Second Specialist’s Meeting on Shielding Aspects of Accelerators, Targets and Irradiation Facilities (SATIF2), 12-13 October 1995, CERN, Geneva, Switzerland, p. 67; P. V. Degtyarenko, M. V. Kossov, H-P. Wellisch, Chiral Invariant Phase Space Event Generator, I. Nucleon-antinucleon annihilation at rest, Eur. Phys. J. **A 8**, p.217 (2000).
42. M. Iodice *et al.*, Performance and results of the RICH detector for kaon physics in Hall A at Jefferson Lab, Proceedings of RICH2004, to be published in Nucl. Instr. and Methods A.
43. JLab experiment E05-009, B. Wojtsekhowski, G. Cates, V. Nelyubin and P. E. Reimer co-spokespersons.
44. http://hallaweb.jlab.org/targets/polhe3/polhe3_tgt.html; and tech notes in <http://www.jlab.org/e94010/>.
45. M. Amarian *et al.*, Phys. Rev. Lett. **89**, 242301 (2002); **92**, 022301 (2004); **93**, 152301 (2004); Z. Meziani, *et al.*, Phys. Lett. B **613**, 148 (2005).
46. W. Xu, *et al.*, Phys. Rev. Lett. **85**, 2900 (2000); F. Xiong, *et al.*, Phys. Rev. Lett. **87**, 242501 (2001).
47. X. Zheng, *et al.*, Phys. Rev. Lett. **92**, 012004 (2004); Phys. Rev. C **70**, 065207 (2004).
48. K. Kramer, *et al.*, Phys. Rev. Lett. **95**, 142002 (2005).
49. JLab E01-012, Spokespersons, J. P. Chen, S. Choi, N. Liyanage.
50. JLab E97-110, Spokespersons, J. P. Chen, A. Deur and F. Garibaldi.
51. E. Babcock, *et al.*, Phys. Rev. Lett. **91**, 123003 (2003).
52. Lai, H.L. *et al.*, Eur. Phys. J. **C12**, 375 (2000).
53. B. A. Kniehl, G. Kramer, and B. Potter, Nucl. Phys. B **582**, 514 (2000).
54. P. Geiger, Ph.D. Dissertation, Ruprecht-Karls-University, Heidelberg (1998).
55. J.L. Friar *et al.*, Phys. Rev. C **42**, 2310 (1990).
56. A. Nogga, Ph. D. thesis, Ruhr-Universität Bochum, Bochum, Germany (2001), p.72.
57. C. Ciofi degli Atti *et al.*, Phys. Rev. C **48**, R968 (1993).

- 58. F. Bissey *et al.*, Phys. Rev. C **64**, 024004 (2001);
- 59. P. Lenisa, and F. Rathmann for the PAX Collaboration, hep-ex/0505054.
- 60. P. R. Bevington and D. K. Robinson, “ Data reduction and error analysis for the physical sciences”, The McGraw-Hill Companies Inc. 1992.